

THESIS

APPLICATION OF SYMBOLIC COMPUTING IN ANALYSIS OF MODAL
PROPERTIES OF STRUCTURALLY COUPLED TWIN TALL BUILDINGS

Submitted by

Eric Lee Richards

Department of Civil and Environmental Engineering

In partial fulfillment of the requirements

For the Degree of Master of Science

Colorado State University

Fort Collins, Colorado

Spring 2011

Master's Committee:

Advisor: Bogusz Bienkiewicz

Marvin Criswell
Scott Shuler

ABSTRACT

APPLICATION OF SYMBOLIC COMPUTING IN ANALYSIS OF MODAL PROPERTIES OF STRUCTURALLY COUPLED TWIN TALL BUILDINGS

This thesis develops non-dimensionalized symbolic expressions for the normalized natural frequencies of two identical tall buildings structurally connected by a skybridge. Symbolic expressions for the modal shapes are also developed to express the coupled movements of the two buildings. The mass and stiffness of the two tall buildings are generalized and reduced to the skybridge level, and the equations of motion are evaluated with Maple 13 math and engineering software. A parametric study of the effects of coupling stiffness on the modal properties is carried out using formulas resulting from symbolic computing. The obtained symbolic expressions are compared with the results of numerical analysis performed using Risa-3D structural engineering analysis software. Findings of this thesis show a good agreement between the symbolic expressions and Risa-3D results. The developed symbolic equations are proposed as a tool for use in the preliminary analysis of tall buildings connected by a skybridge.

ACKNOWLEDGEMENTS

I would like to give sincere thanks and gratitude to my wife. Without her loving support and encouragement through graduate school, none of my accomplishments would have been possible.

I would also like to thank my advisor, Dr. Bogusz Bienkiewicz. Through this process he has continually challenged me to grow and learn and he has also taught me a great deal about ethics and always doing the right thing.

TABLE OF CONTENTS

1. Introduction	1
1.1 Introductory Statements	1
1.2 Scope of Research and Outcomes	2
1.3 Review of Related Literature	3
1.3.1 Symbolic Computing in Engineering	3
1.3.2 Structurally Coupled Buildings	5
2. Background.....	7
2.1 Symbolic Computing in Structural Engineering	7
2.1.1 Definition of Symbolic Computing.....	7
2.1.2 Examples of Symbolic Computing.....	8
2.2 Structurally Coupled Tall Buildings	11
2.2.1 Identical Twin Tall Building Model.....	11
2.2.2 Reduction of Mass and Stiffness to Skybridge Level	13
2.2.3 Free Vibration Analysis of Coupled Twin Tall Buildings	15
3. Analysis of Coupled Twin Tall Building System.....	19
3.1 Development of Equations of Motion for Analysis using Symbolic Computing Tools	20

3.2	Reduction of System from 4 Degrees-of-Freedom to 2 Degrees-of-Freedom	23
3.3	Development of Risa-3D v9.0.1 Structural Analysis Model	26
4.	Results and Discussion	31
4.1	Results from Symbolic Computing	31
4.1.1	Eigenvalue Results	31
4.1.2	Mode Shapes of $y-\theta$ motion.....	33
4.1.3	Uncoupling of $y-\theta$ motion	39
4.2	Numerical Results of Symbolic Equations for 4 Degrees-of-Freedom Reduced to 2 Degrees-of-Freedom	39
4.3	Risa-3D Model Results	41
4.3.1	Comparison of Modal Natural Frequencies	41
4.3.2	Comparison of Modal Shapes	44
5.	Conclusions and Recommendation for Future Research.....	46
	Bibliography	48
	Appendix A.....	52
	Appendix B.....	55
	Appendix C.....	57
	Appendix D.....	60

LIST OF FIGURES

Figure 1. 2DOF spring-mass system.....	9
Figure 2. Isometric view of twin tall buildings connected by a skybridge.	12
Figure 3. Plan view of twin tall building at the skybridge level.....	13
Figure 4. Equivalent system of spring forces reduced to the skybridge level.	14
Figure 5. Plan view of buildings showing fixed-fixed end condition and rigid end sections.	15
Figure 6. Forces due to motion in the x , y and θ -directions.....	16
Figure 7. Free body diagrams for six degrees of freedom in x -, y - and θ -directions.....	17
Figure 8. Risa-3D v9.0.1 Structural Analysis Model Plan View.....	28
Figure 9. Isometric view of Risa-3D v9.0.1 structural analysis model.....	29
Figure 10. Mode shapes for six natural modes determined for twin-tall buildings connected by a skybridge.	35
Figure 11. (a) Schematic showing effective radius of rotation for mode y -out; (b) Schematic showing effective radius of rotation for mode θ -in; (c) Comparison of effective radius of rotation values for coupled mode y - out and θ -in.....	38
Figure 12. Risa-3D v9.0.1 modal shapes for $b=10\text{ m}$ and $E=20000\text{ MPa}$	45

LIST OF TABLES

Table 1. Risa-3D v9.0.1 Member Primary Data for $b = 10\text{ m}$ and $E = 20000\text{ MPa}$	29
Table 2. Risa-3D v9.0.1 General Material Properties for $b = 10\text{ m}$ and $E = 20000$ MPa	30
Table 3. Risa-3D v9.0.1 Joint Coordinates for $b = 10\text{ m}$ and $E = 20000\text{ MPa}$	30
Table 4. Risa-3D v9.0.1 Joint Boundary Conditions for $b = 10\text{ m}$ and $E = 20000$ MPa	30
Table 5. Risa-3D v9.0.1 Joint Loads and Enforced Displacements for $b = 10\text{ m}$ and $E = 20000\text{ MPa}$	30
Table 6. Normalized natural frequency values for y and θ modes with $b = 1.0 \times$ $10 - 9 < l2$ from Maple 13 and Microsoft Excel.....	40
Table 7. Comparison of frequency results of modes θ -in and y -out for parameter b $= 0\text{ m}$ and varying E of the skybridge for thesis equations vs. Risa-3D model.....	43
Table 8. Comparison of frequency results of modes θ -in and y -out for parameter b $= 10\text{ m}$ and varying E of the skybridge for thesis equations vs. Risa-3D model.....	43
Table 9. Comparison of frequency results of modes θ -in and y -out for parameter b $= 20\text{ m}$ and varying E of the skybridge for thesis equations vs. Risa-3D model.....	43

1. Introduction

1.1 Introductory Statements

As the world's population continues to increase and move from rural areas to urban centers, the need for additional working and living space is ever increasing. Due to the high cost of land and the increased number of individuals living in a relatively small space, urban areas have few options to adequately accommodate this increased demand. To accommodate this growing need for physical space, the development of vertical real estate in the form of skyscrapers will be a common solution to alleviate this increased demand. With more and more tall buildings being located in a close proximity, the opportunity exists to connect these structures and create additional physical space. In the creation of the interconnected vertical spaces, the design of these structures will become more sophisticated. It will push designers to extremes and challenge them to incorporate new ideas. The interconnected structures may include, but are not limited to podium structures, sky gardens, or as examined by this thesis, skybridges.

One example of tall buildings or structures connected by a skybridge are the Petronas Towers located in Kuala Lumpur, Malaysia. The towers consist of two 88 story buildings connected by a skybridge spanning 58.4 m (Thornton, Hungspruke, & Joseph, 1997). A unique characteristic about these buildings and their skybridge is the bridge is not engineered to have forces from one building transmitted through the skybridge into the other building (Thornton, Hungspruke, & Joseph, 1997). The bridge is designed to slide or move independent of the buildings, thus not utilizing the skybridge to transfer forces from building to building and allow one building to aide in resistance of forces imposed on the other building (Thornton, Hungspruke, & Joseph, 1997).

1.2 Scope of Research and Outcomes

The modeling of the connection of twin tall towers by a skybridge and the dynamic modal properties of these buildings using free vibration analysis are the focus of research described in this thesis. A set of closed-formed symbolic equations that calculate the natural frequencies and modal shapes of two identical tall buildings connected by a skybridge is developed through the use of the symbolic computing software, Maple 13. This research uses a simplified analytical model with equivalent mass and springs of the representative twin building configuration reduced to the skybridge level, developed by Lim (2008). A comparison is performed to verify the results of the closed-form expressions through the development of a representative model using the structural analysis software, Risa-3D Demonstration version 9.0.1.

In addition, the ultimate intent of this work is to provide designers with a quick and reliable method, for use during the preliminary stages of design of tall buildings, to evaluate the effects and potential benefits of interconnecting such structures. Often designers have to restrain themselves from utilizing the immense amount of computing power in the initial design stages of projects, especially large projects such as super-tall buildings. With the advances in structural analysis software, it is very tempting to immediately start developing a very detailed finite-element model (FEM) that requires a tremendous amount of inputs. Before a highly detailed FEM model that provides the final outputs for design of the building is developed, designers should first develop a very basic, simplified model that is transparent, easily modified and allows the designer to understand the basic workings of the building and its components (Carpinteri, Lacidogna, & Puzzi, 2010). This thesis creates a set of closed-form equations describing the modal

properties of twin tall buildings connected by a skybridge that allow the designer to develop a basic feel for the performance and actions of the building(s) during the preliminary design stages. At this juncture, use of simplified methods is encouraged by well-established designers of tall buildings such as William Baker, partner and structural engineer at Skidmore, Owings and Merrill LLP, the company responsible for structural design of the world's current tallest building (Baker, 2010).

1.3 Review of Related Literature

1.3.1 Symbolic Computing in Engineering

Since its earliest uses and development dating back to 1953, symbolic computing continues to gain popularity (Nolan, 1953). Since that time, the use of symbolic computing software has been used in advanced engineering applications.

There are several distinct advantages related to symbolic analysis of engineering mechanics and structural engineering. Such approaches provide the opportunity to handle algebraic expressions that previously may have reached “unmanageable proportions” and would be too cumbersome to solve by traditional methods (Banerjee, 2004). Symbolic analysis of advanced engineering problems allows the user to focus on the physical nature of the problem and its results. Numerical analysis frequently leads to outcomes that do not allow for direct extraction of physical interpretations of the results (Beltzer, 1990; Sebastian, 2010). It has been noted that the use of symbolic computational software improves the reliability of calculations as well as provides a method to shorten the amount of time required to perform extensive and repetitive calculations (Noor & Andersen, 1979; Beltzer, 1990). Videla et al. (2007) showed that the usage of “Computer algebra systems (CAS)” is capable of reducing computing times involving complex

algebraic equations handled by CAS systems by as much as 50%, e.g. in development of an exact stiffness matrix using the finite element method. The usage of symbolic computation in structural engineering has been used extensively in developing closed-form solutions to engineering problems involving many iterative calculations, the finite-element method, structural analysis, spectral analysis and determination of vibrational frequencies and mode shapes similar to those analyzed in this thesis (Noor & Andersen, 1979; Beltzer, 1990; Pavlovic, 2003; Banerjee, 2004; Videla, Baloa, Griffiths, & Cerrolaza, 2007; Prokic, 2010). As mentioned previously and examined in this thesis, symbolic computing is particularly useful in the analysis of vibrational problems. As shown by Prokic (2006; 2010), symbolic computing programs are commonly used to solve systems of equations and to evaluate the determinants of matrices to determine symbolic forms of eigenvalues. In regards to free vibrational analysis, symbolic computing can be used to quickly, and with more ease than numerical methods, examine the sensitivity of frequencies to changes in physical parameters of the system (Noor & Andersen, 1979). Hashemi and Adique (2010) used symbolic computing software to identify and analyze the coupled vibrational modes that exist within a “sandwich beam” and to evaluate the contributions from the differing modes based on different physical properties of the beam.

Several disadvantages of using symbolic computational software have been noted. The main drawback existing even with today’s advances in technology remains the size, length and complexity of the symbolic results generated by the symbolic software (Noor & Andersen, 1979; Beltzer, 1990). Despite the advances achieved in symbolic computer programs, the display of the results in a compact, reduced and useable format often

requires extensive time and effort by the end user (Noor & Andersen, 1979; Pavlovic, 2003).

A variety of symbolic computing software packages are available for engineering use. Some of the more commonly known programs are Maple version 14, MathCAD version 14, Matlab version R2010b and Mathematica version 8.

1.3.2 Structurally Coupled Buildings

Numerous researchers have looked at the effects and benefits of connecting tall structures through methods such as dampers, skybridges and podiums. The bulk of the research is focused on the use of a physical dampening link between tall structures to reduce the effects of seismic forces. For example, Zhu, Ge and Huang (2010) investigated the effects of connecting two multi-story buildings with either visco-elastic dampers (VED) or viscous fluid dampers (VFD). They found through parametric studies and optimization of results that the use of dampers reduced the base shear of each tower in a twin tower configuration connected by dampers by up to 50%. Kim, Ryu and Chung (2006) also used VEDs connecting three five-story buildings and two twenty-five story buildings of differing structural systems at the seismic joint and with a skybridge, respectively. They found that installing a VED between the top two stories of either set of structures decreased displacements and the number or magnitude of plastic hinges generated within the buildings by a seismic event. Bhaskararao and Jangid (2006) used closed-form analytical expressions and numerical analysis to determine the number and placement of friction dampers to best minimize construction and material cost in order to obtain the highest reduction in building acceleration and displacement. Bharti, Dumne, and Shrimali (2010) looked at the use of Magnetorheological (MR) dampers in three

cases of passive off, passive on, and semi-active control strategies to evaluate the effects on base shear, top floor acceleration and displacement between two structures of differing height. They found the semi-active strategy to be the most effective of the three methods and the impacts on shorter buildings to be more responsive than that of taller buildings, although their findings did show more favorable control of taller structures due to the coupling of the buildings. Lee, Kim and Ko (2010) investigated the connection of a skybridge to two non-identical buildings to determine the best connection configuration for the skybridge. Their findings showed that a rigid connection of the skybridge and the two buildings increased displacements in the top floors of the buildings due to the structural irregularities that existed in the two buildings. Their research also showed that a combination of lead rubber bearings (LRB) and linear motion bearings (LMB) provided the best configuration to control motion of the two connected buildings against seismic and wind forces. Various research has been done to investigate the impacts of utilizing passive, semi-active and active dampers when connecting two buildings in close proximity. The general consensus resulting from these studies is that semi-active dampers represent the best and most economical solutions for mitigation of building vibrations (Asano, Yamano, Yoshie, Koike, Nakagawa, & Murata, 2003; Christenson, Spencer Jr., Johnson, & Seto, 2006; Christenson, Spencer Jr., & Johnson, 2007).

The analysis of multiple structures connected by some linkage, whether a podium structure, sky garden or skybridge, is more complex for seismic and wind loads than that of single tall structures under the same loading. The research mentioned above was predominantly focused on building response caused by seismic loading. Research has also been carried out to investigate wind effects on structures and analyze the coupled

vibrational motions resulting from structural linkages. Wind tunnel studies have been conducted to provide insight and to clarify the complicated methods needed to properly analyze multiple-connected structures, and to develop the wind forces on the structures, and how those are affected by the buildings' coupled interactions (Boggs & Hosoya, 2001; Rofail & Holmes, 2007; Lim & Bienkiewicz, 2007).

The coupled vibrational modes discussed in this thesis also occur in other engineering structures. Representative examples of such structures are long-span bridges, “sandwiched beams”, and other engineering structural systems (Sepe & Augusti, 2001; Sepe, Diaferio, & Augusti, 2003; Banerjee, 2004; Hashemi & Adique, 2010).

2. Background

2.1 Symbolic Computing in Structural Engineering

2.1.1 Definition of Symbolic Computing

A definition provided for symbolic computation as found on the website

Wikipedia states:

Symbolic computation or algebraic computation, relates to the use of machines, such as computers, to manipulate mathematical equations and expressions in symbolic form, as opposed to manipulating the approximations of specific numerical quantities represented by those symbols. (Symbolic Computation, 2010)

Explained further, symbolic computing in its simplest form is a computer algorithm that requires input from the user consisting of either numerical values or exact terms such as “fractions, radicals, and symbols” and then performs mathematical operations on the numeric values and symbols provided by the user (Maple). The fractions and radicals may contain numerical quantities, whole number integers, or symbols. The advantage of

symbolic computing technology is how these algorithms handle non-numeric terms. The computer algorithm is coded in such a manner that by entering particular inputs, namely the use of numeric terms and symbols representative of numeric values, calculations are performed using the numbers and symbols defined by the user and carried through each step of the calculation until a final answer is determined or the user assigns numerical values to the symbols. If no numeric values are used and only symbols are input, then the program displays outputs as exact values with no numerical simplification and consequently no rounding errors.

The basic concept of symbolic computing is that generic symbols representative of numeric quantities are used to perform algebraic calculations without using numeric values until desired by the user. While each proprietary software has its own specific syntax, all symbolic software packages operate under this basic principle.

2.1.2 Examples of Symbolic Computing

A representative example of software capable of performing both numerical and symbolic calculations is Wolfram's Mathematica 8. Within this software, as with other symbolic computing programs, the user may perform standard numerical calculations as would be performed on a basic calculator. Several examples outlined from Wolfram's website are:

$$\text{Input}[1] := 24 + 35 - 6 \quad [1]$$

$$\text{Output}[1] = 53 \quad [2]$$

or

$$\text{Input}[2] := 63 \times 857 \div 3 \quad [3]$$

$$\text{Output}[2] = 17997 \quad [4]$$

Both sets of inputs and outputs demonstrate how a user may input numerical values within the software and how a numerical answer is returned, which in these two cases happen to be the exact output. Similarly, if the user specifies an algebraic expression with an unknown variable x , this can also be handled by the software. For example:

$$\text{Input}[3] := 3x - 5x^2 + 7 \quad [5]$$

$$\text{Output}[3] = 7 + 3x - 5x^2 \quad [6]$$

No simplification is able to be performed and the output is the same as the input.

Example 4 illustrates a case when simplification can be implemented:

$$\text{Input}[4] := 7x^2 - 2x + 4x^2 + 3x - 2 \quad [7]$$

$$\text{Output}[4] = 11x^2 + x - 2 \quad [8]$$

As can be seen from the output in equation 8, the software easily handles the algebraic simplification of equation 7 according to standard rules. More advanced problems can be evaluated as well. A representative example is determining the eigenvalues and eigenvectors of a two degree-of-freedom (2DOF) mass and spring system using free vibration analysis, see Figure 1.

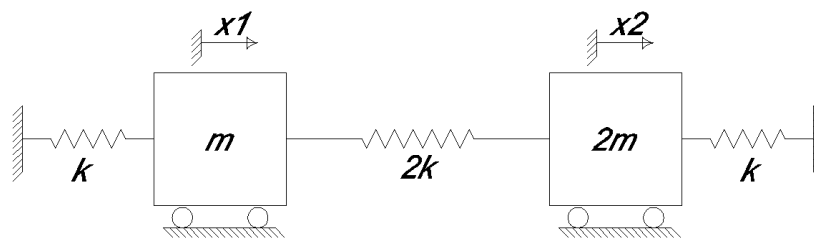


Figure 1. 2DOF spring-mass system

The equations of free motion for this system are:

$$m\ddot{x}_1 + 3kx_1 - 2kx_2 = 0 \quad [9]$$

$$2m\ddot{x}_2 - 2kx_1 + 3kx_2 = 0 \quad [10]$$

Assuming that $x_1 = A_1 e^{i\omega t}$ and $x_2 = A_2 e^{i\omega t}$, equations 9 and 10 are converted into a set of two algebraic homogeneous equations written in matrix form:

$$\begin{bmatrix} (3k - m\omega^2) & -2k \\ -2k & (3k - 2m\omega^2) \end{bmatrix} \begin{Bmatrix} A_1 \\ A_2 \end{Bmatrix} = \begin{Bmatrix} 0 \\ 0 \end{Bmatrix} \quad [11]$$

Pre-multiplying row 1 by $1/m$ and row 2 by $1/2m$ and letting $\omega^2 = \lambda$ result in the following equation:

$$\begin{bmatrix} \left(\frac{3k}{m} - \lambda\right) & -\frac{2k}{m} \\ -\frac{k}{m} & \left(\frac{3k}{2m} - \lambda\right) \end{bmatrix} \begin{Bmatrix} A_1 \\ A_2 \end{Bmatrix} = \begin{Bmatrix} 0 \\ 0 \end{Bmatrix} \quad [12]$$

Determination of the eigenvalues and eigenvectors of equation 12 is a simple and straight forward procedure. With the aid of symbolic computer algebra software such as Mathematica 8 or Maple 13, it can also easily be accomplished. For example, if Maple 13 is used, the following sequences are formulated as input:

$$A := \begin{bmatrix} \frac{3k}{m} & -\frac{2k}{m} \\ \frac{k}{m} & \frac{3k}{2m} \end{bmatrix} \quad [13]$$

with(LinearAlgebra): [14]

v, e := Eigenvectors(A) [15]

The output is as follows:

$$v, e := \begin{bmatrix} \frac{\left(\frac{9}{4} + \frac{1}{4}\sqrt{41}\right)k}{m} \\ \frac{\left(\frac{9}{4} - \frac{1}{4}\sqrt{41}\right)k}{m} \end{bmatrix}, \begin{bmatrix} -\frac{2k}{\left(\frac{9}{4} + \frac{1}{4}\sqrt{41}\right)k - 3k} & -\frac{2k}{\left(\frac{9}{4} - \frac{1}{4}\sqrt{41}\right)k - 3k} \\ 1 & 1 \end{bmatrix} \quad [16]$$

As can be seen from equation 13, the $(-\lambda)$ term is not input into matrix $[A]$. This results from the code or general format in which eigenvector problems are solved by Maple 13.

According to the help menu within Maple 13, the “*Eigenvectors(.)*” function solves the

simple eigenvector problem $A \cdot x = \lambda \cdot x$ where A refers to the matrix similar to that shown in equation 13, x refers to the vector $x^T = \{A_1 \ A_2\}$ (shown here transposed) as displayed in equation 12, λ refers to the matrix:

$$\lambda = \begin{bmatrix} \lambda & 1 \\ 1 & \lambda \end{bmatrix} \quad [17]$$

and the $(.)$ is the operator syntax within Maple 13 signifying the multiplication of matrix $[A]$ or matrix $[\lambda]$ by vector $\{x\}$. Therefore, the software is coded to automatically solve for the λ values when the command "*Eigenvectors(..)*" is called. The command "*with(LinearAlgebra):*" shown in equation 14 is a command within Maple 13 that indicates the user needs to access the linear algebra package to perform operations such as to "construct and manipulate Matrices and Vectors, compute standard operations, query results and solve linear algebra problems," as outlined in the Maple 13 help menu.

The results in equation 16 show the output for the eigenvalues and eigenvectors of the 2DOF problem displayed in Figure 1. The first answer in brackets displays the two eigenvalues that exist for this problem displaying the symbols used and no numerical simplification. The second set of answers displayed in brackets are eigenvectors determined for the two eigenvalues with the expression in column one corresponding to the first eigenvalue and that in column two to the second eigenvalue. Again, the representative symbols are carried through the calculations and displayed in the final answer with no simplification.

2.2 Structurally Coupled Tall Buildings

2.2.1 Identical Twin Tall Building Model

Using the building configuration defined in Lim (2008) as a guide, an identical twin tall building configuration is utilized for this thesis as shown in Figure 2.

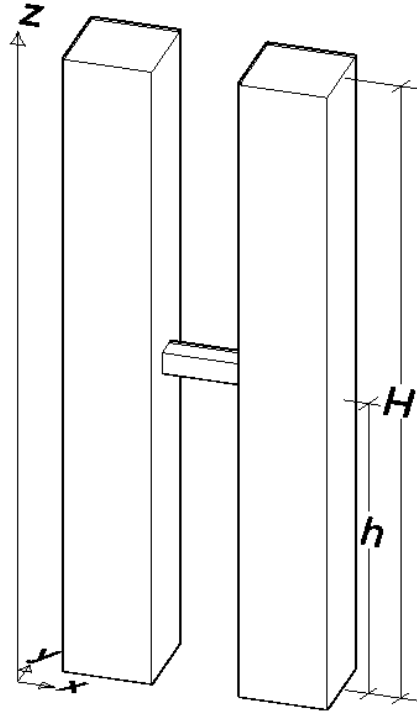


Figure 2. Isometric view of twin tall buildings connected by a skybridge.

A plan view of the twin buildings, at the skybridge level, is shown in Figure 3. The local coordinates for each building and the planar dimension D of the square cross-section are included in the figure. The building on the left is denoted as $B1$ and the building on the right as $B2$. The mass of each building is assumed to be distributed uniformly throughout the cross-section of the building and therefore the center of mass is assumed at the geometric center of each building and denoted as the origin (O). The stiffness of each building is also assumed to concentrically pass through the geometric center of each cross-section. As a result, the dynamic and static couplings of the buildings are eliminated (Thomson & Dahleh, 1998).

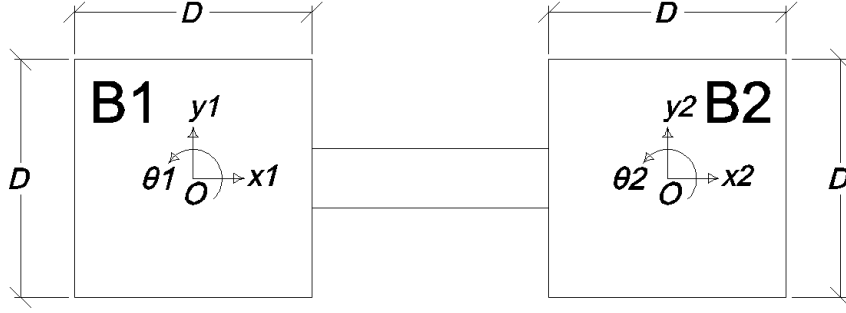


Figure 3. Plan view of twin tall building at the skybridge level

2.2.2 Reduction of Mass and Stiffness to Skybridge Level

The equations for mass reduced to the skybridge level, developed in Lim (2008), are used in this thesis for the mass in the sway directions x and y and the torsional direction θ . A simplification is used by assuming a single linear mode approximation of the building vibration in each direction.

$$m_x^e = m_x^* \left(\frac{H}{h}\right)^2, m_y^e = m_y^* \left(\frac{H}{h}\right)^2, m_\theta^e = m_\theta^* \left(\frac{H}{h}\right)^2 \quad [18]$$

where

$$m_x^* = \frac{m_x H}{3}, m_y^* = \frac{m_y H}{3}, m_\theta^* = \frac{m_\theta H}{3} \quad [19]$$

$$m_x = m_y = \rho_m D^2, m_\theta = \rho_m D^2 r_o^2 \quad [20]$$

As assumed in Lim (2008), m_x, m_y and m_θ are the constant mass (or polar mass moment of inertia) per unit height, ρ_m is the building mass density and r_o is the radius of gyration about the mass center (O). A full derivation of the equations used in Lim (2008) is presented in Appendix A. The final form for the equations for equivalent mass is as follows (equations A-33 and A-35 in Appendix A):

$$m_x^e = m_y^e = \frac{\rho_m D^2 H^3}{3h^2} \quad [21]$$

$$m_{\theta}^e = \frac{\rho_m D^2 H^3}{3h^2} \left(\frac{h r_0^2}{H} \right) \quad [22]$$

Using the model developed in Lim (2008), a system with equivalent spring forces reduced to the skybridge level is used as a basis for determining the equations of motion for the twin building system (equation A-29 in Appendix A).

$$k_x^e = m_x^e \omega_x^2 = \frac{\rho_m D^2 H^3}{3h^2} (2\pi f_x)^2 \quad \text{and} \quad k_y^e = m_y^e \omega_y^2 = \frac{\rho_m D^2 H^3}{3h^2} (2\pi f_y)^2 \quad [23]$$

$$k_{\theta}^e = m_{\theta}^e \omega_{\theta}^2 = \frac{\rho_m D^2 H^3}{3h^2} \left(\frac{h r_0^2}{H} \right) (2\pi f_{\theta})^2 \quad [24]$$

where ω_x , ω_y and ω_{θ} are the circular natural frequencies of the buildings in their respective directions.

As can be seen from equation 24, the formula for m_{θ}^e can be rewritten as:

$$k_{\theta}^e = m_{\theta}^e \omega_{\theta}^2 = m_x^e \left(\frac{h r_0^2}{H} \right) (2\pi f_{\theta})^2 \quad \text{or} \quad m_y^e \left(\frac{h r_0^2}{H} \right) (2\pi f_{\theta})^2 \quad [25]$$

Figure 4 shows a schematic of the equivalent spring forces represented in the coupled building system. Sway stiffness in the x - and y -directions are shown for each building $B1$ and $B2$ as are the torsional stiffnesses.

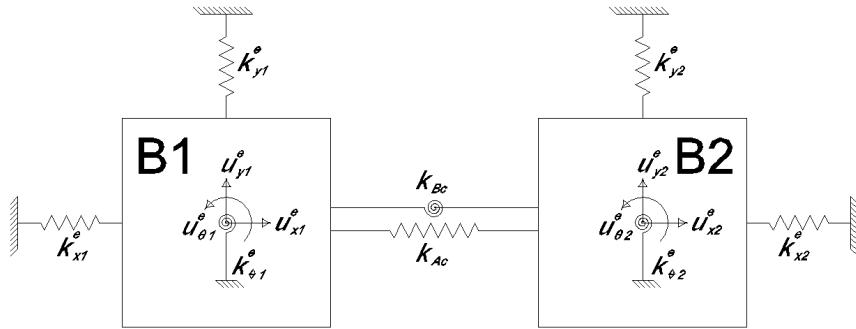


Figure 4. Equivalent system of spring forces reduced to the skybridge level.

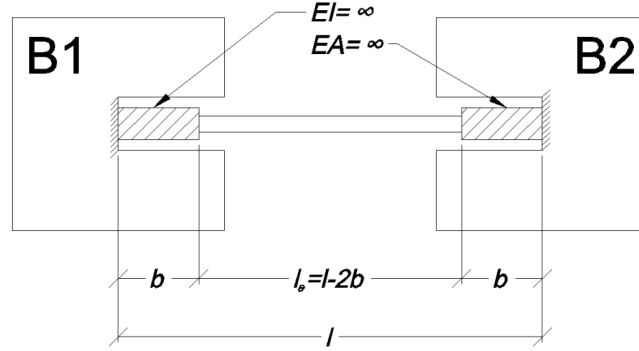
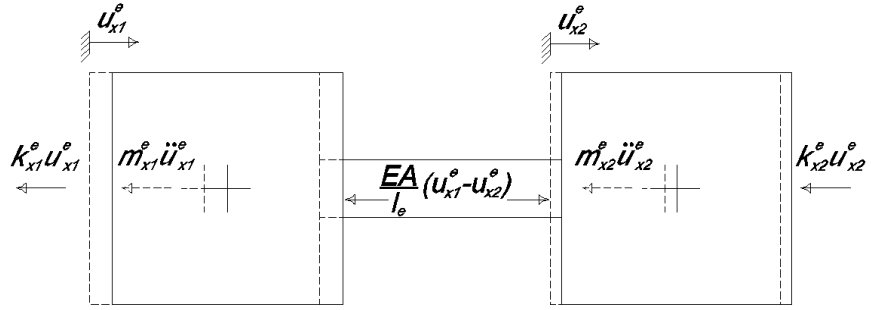


Figure 5. Plan view of buildings showing fixed-fixed end condition and rigid end sections.

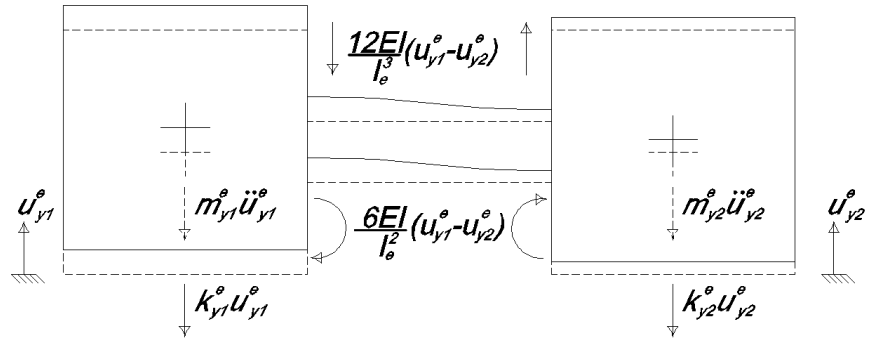
Also shown in Figure 4 are a linear spring and a torsional spring labeled k_{Ac} and k_{Bc} respectively, representing axial and bending coupling stiffness due to the skybridge. Figure 5 shows a plan view of the two buildings (at the skybridge level) with the skybridge modeled as a fixed-fixed beam. Also shown in Figure 5 are rigid end sections of the skybridge modeled with infinite axial and bending stiffness (Lim, 2008). The rigid end sections represent stiffening assumed to exist due to an engineered connection of the skybridge at the building's central core and stiffening from connections along the building/skybridge interface. Therefore, the linear spring in Figure 4 represents the axial stiffness of the skybridge and its equation is $k_{Ac} = EA/l_e$ where E is the effective modulus of elasticity of the bridge, A is the effective area of the bridge, and $l_e = l - 2b$ is the effective length of the skybridge. Similarly, the torsional spring at the skybridge in Figure 4 represents the bending stiffness of the skybridge $k_{Bc} = EI/l_e^3$ where I is the area moment of inertia of the skybridge cross section.

2.2.3 Free Vibration Analysis of Coupled Twin Tall Buildings

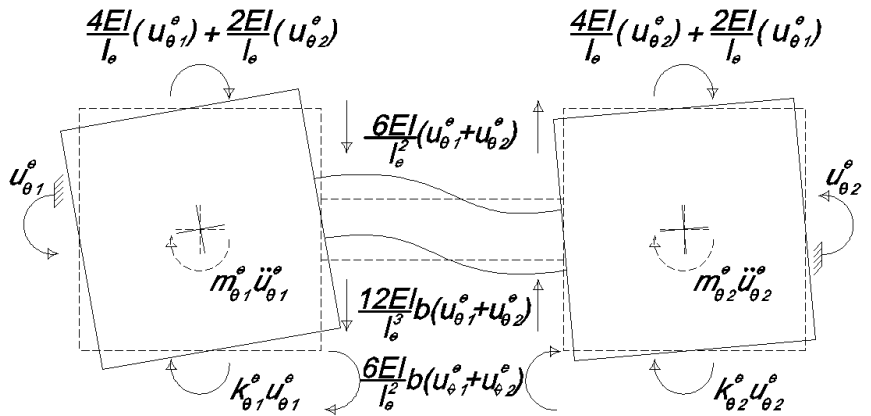
Using the equivalent spring forces shown in Figure 4, the rigid end links of length b , and the effective length l_e , the equations of motion are determined for the x -, y - and θ -directions for the twin towers (Meriam & Kraige, 2002). Figure 6 shows the resulting



(a) Forces due to motion in the x -direction.



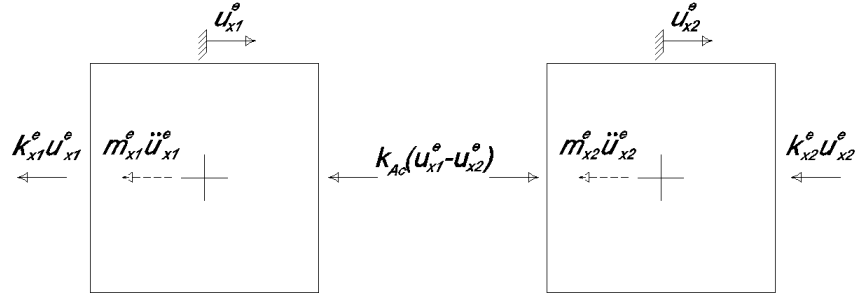
(b) Forces due to motion in the y -direction.



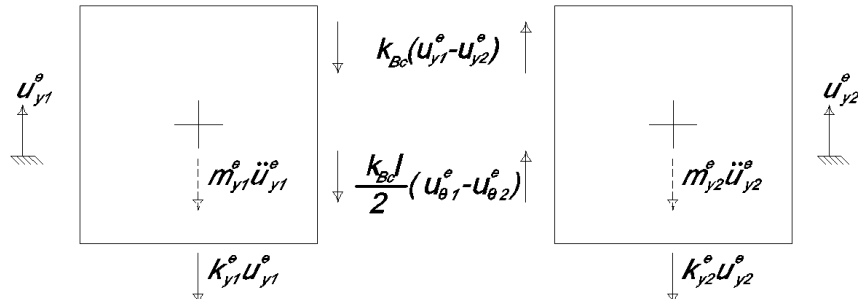
(c) Forces due to motion in the θ -direction.

Figure 6. Forces due to motion in the x , y and θ -directions

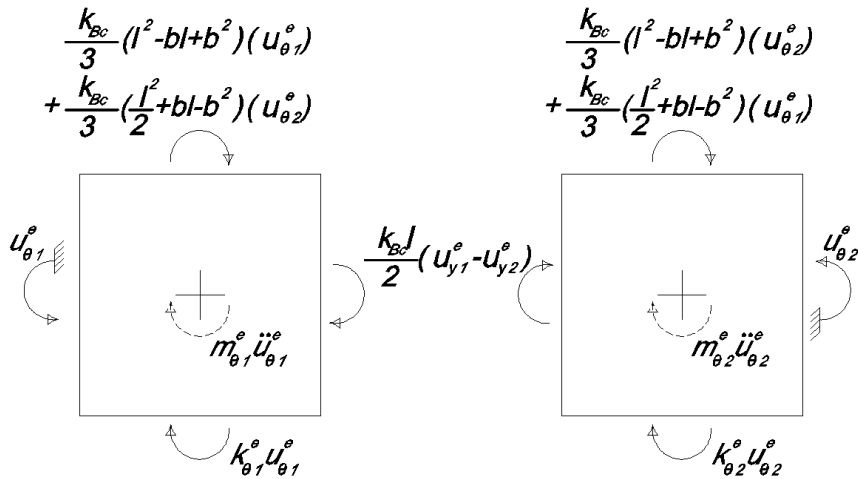
forces from motion in the three differing directions. In Figure 6 (a), assuming the movement of building B1 is greater than B2, the resulting forces of each building are shown. Likewise for Figure 6 (b) and Figure 6 (c), it is assumed that the motion of



(a) Free body diagram of forces in the x -direction



(b) Free body diagram of forces in the y -direction



(c) Free body diagram of forces in the θ -direction

Figure 7. Free body diagrams for six degrees of freedom in x -, y - and θ -directions

building B1 is greater than B2 in the sway and torsional movement respectively, and the resulting forces are thusly shown. Figure 6 (c) also shows shear and moment forces induced at the end of the rigid end sections of the skybridge due to rotation of the buildings.

Substituting k_{Ac} and k_{Bc} into the equations of Figure 6 results in the free body diagrams, for forces summed in the x -, y - and θ -directions, depicted in Figure 7.

Appendix B shows the complete derivation of the forces displayed in Figure 6 and Figure 7. From the free body diagrams in Figure 7, the resulting equations of motion from free vibration analysis in the x -direction are as follows:

$$m_x^e \ddot{u}_{x1}^e(t) + (k_x^e + k_{Ac})u_{x1}^e(t) - k_{Ac}u_{x2}^e(t) = 0 \quad [26]$$

$$m_x^e \ddot{u}_{x2}^e(t) - k_{Ac}u_{x1}^e(t) + (k_x^e + k_{Ac})u_{x2}^e(t) = 0 \quad [27]$$

It should be noted that the configuration of the skybridge for this thesis assumes that, when the buildings and skybridge are viewed in an elevation view or isometric view as shown in Figure 2, the skybridge has a pinned connection at each end of the skybridge in the direction perpendicular to the longitudinal axis of the skybridge. Therefore, as both buildings move in either direction along the x -axis, the bridge will rotate about the y -axis and no shear forces or bending moments induced into the building/bridge system result from these motions.

As can be seen from the equations displayed in Figure 7 (b) and (c) and derived in Appendix B, coupling exists between the y - and θ -directions, resulting in the following equations of motion in the y -direction:

$$m_y^e \ddot{u}_{y1}^e(t) + (k_y^e + k_{Bc})u_{y1}^e(t) - k_{Bc}u_{y2}^e(t) + k_{Bc} \frac{l}{2} u_{\theta1}^e(t) + k_{Bc} \frac{l}{2} u_{\theta2}^e(t) = 0 \quad [28]$$

$$m_y^e \ddot{u}_{y2}^e(t) - k_{Bc} u_{y1}^e(t) + (k_y^e + k_{Bc}) u_{y2}^e(t) - k_{Bc} \frac{l}{2} u_{\theta 1}^e(t) - k_{Bc} \frac{l}{2} u_{\theta 2}^e(t) = 0 \quad [29]$$

Likewise, the equations of motion in the θ -direction are:

$$m_\theta^e \ddot{u}_{\theta 1}^e(t) + k_{Bc} \frac{l}{2} u_{y1}^e(t) - k_{Bc} \frac{l}{2} u_{y2}^e(t) + \left[k_\theta^e + \frac{k_{Bc}}{3} (l^2 - bl + b^2) \right] u_{\theta 1}^e(t) + \left[\frac{k_{Bc}}{3} \left(\frac{l^2}{2} + bl - b^2 \right) \right] u_{\theta 2}^e(t) = 0 \quad [30]$$

$$m_\theta^e \ddot{u}_{\theta 2}^e(t) + k_{Bc} \frac{l}{2} u_{y1}^e(t) - k_{Bc} \frac{l}{2} u_{y2}^e(t) + \left[\frac{k_{Bc}}{3} \left(\frac{l^2}{2} + bl - b^2 \right) \right] u_{\theta 1}^e(t) + \left[k_\theta^e + \frac{k_{Bc}}{3} (l^2 - bl + b^2) \right] u_{\theta 2}^e(t) = 0 \quad [31]$$

3. Analysis of Coupled Twin Tall Building System

The analysis of the coupled twin tall building system consists of manipulation of the equations of motion such that the eigenvalues and eigenvectors of the system can be determined through the use of symbolic computing tools. The results of this analysis are a set of closed-form symbolic expressions for both the eigenvalue and eigenvector solutions. The ultimate goal of this analysis is to develop the formulas in such a way that the final results are shown in a non-dimensionalized form thus allowing for wider application. Analysis includes a limiting case of an infinitely stiff skybridge and illustrates how the computed dynamic properties are affected while the stiffness is approaching the limit. Lastly, a Risa-3D model is created using assumed properties of the building system and results from this structural analysis software are determined. These results are compared with numerical values determined from the symbolic solutions - the eigenvalues and eigenvectors - using the same properties. Two specific properties are varied for the Risa-3D model and the numerical evaluation of the symbolic equations. The parameter b is varied for lengths 0 m, 10 m and 20 m and the modulus of elasticity

of the skybridge is varied for values of 5,000 MPa, 10,000 MPa and 20,000 MPa to evaluate the performance of the building system with the varying lengths of the rigid end sections and varying stiffness of the skybridge.

3.1 Development of Equations of Motion for Analysis using Symbolic Computing Tools

It can be seen from equations 26 and 27 that the dynamic motions of the buildings in the x -direction are decoupled from those in the y - and θ -directions. Therefore the equations of motion in the x -direction can be placed into the following representative 2DOF matrix expression:

$$[m^e]_x \{\ddot{u}^e\}_x + [k^e]_x \{u^e\}_x = 0 \quad [32]$$

where

$$[m^e]_x = \begin{bmatrix} m_x^e & 0 \\ 0 & m_x^e \end{bmatrix} \quad [33]$$

$$[k^e]_x = k_x^e \begin{bmatrix} 1 + \psi_A & -\psi_A \\ -\psi_A & 1 + \psi_A \end{bmatrix} \quad [34]$$

$$\psi_A = \frac{k_{Ac}}{k_x^e} = \text{relative axial stiffness} \quad [35]$$

$$\{u^e\}_x = \begin{Bmatrix} u_{x1}^e \\ u_{x2}^e \end{Bmatrix} \quad [36]$$

Equation 32 is similar to the 2DOF example presented in Section 2.1.2. It can be explicitly written as follows:

$$\frac{-m_x^e \omega^2}{k_x^e} \begin{bmatrix} 1 & 0 \\ 0 & 1 \end{bmatrix} \begin{Bmatrix} u_{x1}^e \\ u_{x2}^e \end{Bmatrix} + \begin{bmatrix} 1 + \psi_A & -\psi_A \\ -\psi_A & 1 + \psi_A \end{bmatrix} \begin{Bmatrix} u_{x1}^e \\ u_{x2}^e \end{Bmatrix} = \{0\} \quad [37]$$

Denoting $m_x^e \omega^2 / k_x^e = \lambda$, equation 37 can be expressed in a non-dimensionalized form suitable for analysis by the symbolic computing software:

$$\begin{bmatrix} 1 + \psi_A - \lambda & -\psi_A \\ -\psi_A & 1 + \psi_A - \lambda \end{bmatrix} \begin{Bmatrix} \frac{u_{x1}^e}{D} \\ \frac{u_{x2}^e}{D} \end{Bmatrix} = \{0\} \quad [38]$$

Examination of equations 28 through 31 shows the forces from the y - and θ -directions are coupled. They form a coupled four degree-of-freedom (4DOF) system defined by the following equation:

$$[m^e]_{y\theta} \{\ddot{u}^e\}_{y\theta} + [k^e]_{y\theta} \{u^e\}_{y\theta} = \{0\} \quad [39]$$

where

$$[m^e]_{y\theta} = \begin{bmatrix} m_y^e & 0 & 0 & 0 \\ 0 & m_y^e & 0 & 0 \\ 0 & 0 & m_\theta^e & 0 \\ 0 & 0 & 0 & m_\theta^e \end{bmatrix} \quad [40]$$

$$[k^e]_{y\theta} = k_y^e \begin{bmatrix} 1 + \psi_B & -\psi_B & \psi_B \frac{l}{2} & \psi_B \frac{l}{2} \\ -\psi_B & 1 + \psi_B & -\psi_B \frac{l}{2} & -\psi_B \frac{l}{2} \\ \psi_B \frac{l}{2} & -\psi_B \frac{l}{2} & \frac{k_\theta^e}{k_y^e} + \frac{\psi_B}{3} (l^2 - bl + b^2) & \frac{\psi_B}{3} \left(\frac{l^2}{2} + bl - b^2 \right) \\ \psi_B \frac{l}{2} & -\psi_B \frac{l}{2} & \frac{\psi_B}{3} \left(\frac{l^2}{2} + bl - b^2 \right) & \frac{k_\theta^e}{k_y^e} + \frac{\psi_B}{3} (l^2 - bl + b^2) \end{bmatrix} \quad [41]$$

$$\psi_B = \frac{k_{BC}}{k_y^e} = \text{relative bending stiffness} \quad [42]$$

$$\{u^e\}_{y\theta} = \begin{Bmatrix} u_{y1}^e \\ u_{y2}^e \\ u_{\theta 1}^e \\ u_{\theta 2}^e \end{Bmatrix} \quad [43]$$

Recall that l and b are, respectively, the length from the geometric center of building B1 to the geometric center of building B2 and the length of the infinitely rigid portions of the skybridge. The relative bending stiffness ψ_B is used as a parameter indicating the level of structural coupling between the skybridge and the building. This

parameter is changed while the effects of its value on the dynamic properties of the coupled system are evaluated.

It is necessary to manipulate equation 39 to resemble an expression similar to that of equation 38 determined for the x -direction so the dynamic modal properties may be determined with the symbolic computing software. A complete derivation of the simplification of terms and steps needed to change equation 39 into its non-dimensionalized format (to be evaluated by the symbolic computing software) can be found in the Appendix C. The resulting form is as follows:

$$-\lambda[I]_{y\theta}\{U^e\}_{y\theta} + [S^e]_{y\theta}\{U^e\}_{y\theta} = \{0\} \quad [44]$$

where

$$\lambda = \frac{\omega^2}{k_y^e/m_y^e} = \frac{\omega^2}{\omega_{y,ref}^2} \quad [45]$$

$$[I]_{y\theta} = \begin{bmatrix} 1 & 0 & 0 & 0 \\ 0 & 1 & 0 & 0 \\ 0 & 0 & 1 & 0 \\ 0 & 0 & 0 & 1 \end{bmatrix} \quad [46]$$

$$[S^e]_{y\theta} = \begin{bmatrix} 1 + \psi_B & -\psi_B & \psi_B \alpha_1 & \psi_B \alpha_1 \\ -\psi_B & 1 + \psi_B & -\psi_B \alpha_1 & -\psi_B \alpha_1 \\ \psi_B \alpha_1 & -\psi_B \alpha_1 & \kappa + \psi_B \alpha_2 & \psi_B \alpha_3 \\ \psi_B \alpha_1 & -\psi_B \alpha_1 & \psi_B \alpha_3 & \kappa + \psi_B \alpha_2 \end{bmatrix} \quad [47]$$

$$\{U^e\}_{y\theta} = \begin{pmatrix} \frac{u_{y1}^e}{D} \\ \frac{u_{y2}^e}{D} \\ \frac{u_{\theta1}^e H r_o}{D h} \\ \frac{u_{\theta2}^e H r_o}{D h} \end{pmatrix} \quad [48]$$

$$\kappa = \frac{k_\theta^e}{k_y^e r_o^2} \quad [49]$$

$$\alpha_1 = \frac{l}{2 r_o} \quad [50]$$

$$\alpha_2 = \frac{l^2 - bl + b^2}{3 r_o^2} \quad [51]$$

$$\alpha_3 = \frac{l^2/2 + bl - b^2}{3 r_o^2} \quad [52]$$

The final equation to be used in eigenvalue analysis using the symbolic computing software is:

$$\begin{bmatrix} 1 + \psi_B - \lambda & -\psi_B & \psi_B \alpha_1 & \psi_B \alpha_1 \\ -\psi_B & 1 + \psi_B - \lambda & -\psi_B \alpha_1 & -\psi_B \alpha_1 \\ \psi_B \alpha_1 & -\psi_B \alpha_1 & \kappa + \psi_B \alpha_2 - \lambda & \psi_B \alpha_3 \\ \psi_B \alpha_1 & -\psi_B \alpha_1 & \psi_B \alpha_3 & \kappa + \psi_B \alpha_2 - \lambda \end{bmatrix} \begin{Bmatrix} \frac{u_{y1}^e}{D} \\ \frac{u_{y2}^e}{D} \\ \frac{u_{\theta 1}^e H r_o}{D h} \\ \frac{u_{\theta 2}^e H r_o}{D h} \end{Bmatrix} = \{0\} \quad [53]$$

3.2 Reduction of System from 4 Degrees-of-Freedom to 2 Degrees-of-Freedom

Analysis was performed for a hypothetical case of the coupled twin tall building system as the lengths b of the skybridge rigid ends increase until both equal a final value of $l/2$. Observation of the system as the length b parameter approaches $l/2$ shows that the skybridge resembles a rigid body and thusly the twin-building system reduces from 4DOF to 2DOF. This problem is similar to that explored by Schlichting (1979) in his discussion of a “mathematical analog of a boundary-layer flow” initially introduced by L. Prandtl. The example discusses damped vibration of a point-mass described by second order linear differential equations and examines how the solution to the equation changes when the value of the mass is reduced to a very small value. This case is compared with a massless system. Schlichting (1979) applied this example to illustrate a boundary-layer theory in presence of small fluid viscosity and that with viscosity set to be exactly equal to zero. The near solid surface flows are completely different in the two cases. A similar

scenario is posed here as there is a significant difference in the dynamic responses of the systems when parameter b is less than $l/2$ (4DOF) and when it is at the limit of $= l/2$ (2DOF).

To determine the resulting mode shapes of the final 2DOF system, analysis of the system as b approaches the limit of $l/2$ is needed. Starting with equation 39 and substituting the values for m_y^e and m_θ^e into the mass matrix and extracting the ψ_B term from the stiffness matrix, the following equation is obtained:

$$\begin{aligned}
 & \begin{bmatrix} m_y^e & 0 & 0 & 0 \\ 0 & m_y^e & 0 & 0 \\ 0 & 0 & m_y^e \left(\frac{h}{H}\right) r_0^2 & 0 \\ 0 & 0 & 0 & m_y^e \left(\frac{h}{H}\right) r_0^2 \end{bmatrix} \begin{Bmatrix} \ddot{u}_{y1}^e \\ \ddot{u}_{y2}^e \\ \ddot{u}_{\theta 1}^e \\ \ddot{u}_{\theta 2}^e \end{Bmatrix} \\
 & + k_y^e \psi_B \begin{bmatrix} \frac{1}{\psi_B} + 1 & -1 & & \frac{l}{2} \\ -1 & \frac{1}{\psi_B} + 1 & & -\frac{l}{2} \\ \frac{l}{2} & -\frac{l}{2} & \frac{k_\theta}{\psi_B k_y} + \frac{1}{3}(l^2 - bl + b^2) & \frac{1}{3}\left(\frac{l^2}{2} + bl - b^2\right) \\ \frac{l}{2} & -\frac{l}{2} & \frac{1}{3}\left(\frac{l^2}{2} + bl - b^2\right) & \frac{k_\theta}{\psi_B k_y} + \frac{1}{3}(l^2 - bl + b^2) \end{bmatrix} \begin{Bmatrix} u_{y1}^e \\ u_{y2}^e \\ u_{\theta 1}^e \\ u_{\theta 2}^e \end{Bmatrix} \\
 & = \{0\}
 \end{aligned} \tag{54}$$

It can be seen that as parameter b approaches $l/2$, the value of ψ_B approaches infinity.

As ψ_B tends to infinity, the quantities within the mass matrix still have finite values as do the values in the force vector; therefore the values within the stiffness matrix must be finite to ensure that equation [54] is satisfied for a nontrivial solution. Therefore, the four equations within the stiffness matrix must equal:

$$u_{y1}^e - u_{y2}^e + \frac{l}{2}(u_{\theta 1}^e + u_{\theta 2}^e) = 0 \tag{55}$$

$$-u_{y1}^e + u_{y2}^e - \frac{l}{2}(u_{\theta 1}^e + u_{\theta 2}^e) = 0 \tag{56}$$

$$\frac{l}{2}(u_{y1}^e - u_{y2}^e) + \frac{1}{3}(l^2 - bl + b^2)u_{\theta1}^e + \frac{1}{3}\left(\frac{l^2}{2} + bl - b^2\right)u_{\theta2}^e = 0 \quad [57]$$

$$\frac{l}{2}(u_{y1}^e - u_{y2}^e) + \frac{1}{3}\left(\frac{l^2}{2} + bl - b^2\right)u_{\theta1}^e + \frac{1}{3}(l^2 - bl + b^2)u_{\theta2}^e = 0 \quad [58]$$

Multiplying equation 56 by (-1) results in the same expression as equation 55, thus equations 55 and 56 are the same. Pre-multiplying equation 57 and 58 by $2/l$ and substituting $b = l/2$ results in the same equations as was found for equation 55:

$$u_{y1}^e - u_{y2}^e + \frac{l}{2}(u_{\theta1}^e + u_{\theta2}^e) = 0 \quad [59]$$

Therefore, at $b = l/2$ all 4 equations are the same. Next, assume that:

$$y = \frac{u_{y1}^e + u_{y2}^e}{2} \rightarrow 2y = u_{y1}^e + u_{y2}^e \quad [60]$$

$$\theta = \frac{u_{\theta1}^e + u_{\theta2}^e}{2} \rightarrow 2\theta = u_{\theta1}^e + u_{\theta2}^e \quad [61]$$

Substitute equation 61 into 59:

$$u_{y1}^e - u_{y2}^e + l\theta = 0 \quad [62]$$

Solve equation 60 for u_{y2}^e and substitute into equation 62 and solve for u_{y1}^e to get:

$$u_{y1}^e = y - \frac{l}{2}\theta \quad [63]$$

Likewise:

$$u_{y2}^e = y + \frac{l}{2}\theta \quad [64]$$

If it is assumed that $y \neq 0$ and $\theta = 0$, then from equations 63 and 64:

$$u_{y1}^e = u_{y2}^e \quad [65]$$

Similarly, if it is assumed that $\theta \neq 0$ and $y = 0$, then from equations 63 and 64:

$$u_{y1}^e = -\frac{l}{2}\theta, u_{y2}^e = \frac{l}{2}\theta \quad [66]$$

From the formulas in equations 65 and 66, a pure translational mode shape in the y -direction exists as does a mode shape with coupled rotational and translational motion.

Thus the two modes shapes now present in the 2DOF system are:

$$\{\phi\}_{y,in} = \begin{Bmatrix} 1 \\ 1 \\ 0 \\ 0 \end{Bmatrix} \quad [67]$$

$$\{\phi\}_{\theta,in} = \begin{Bmatrix} -\frac{l}{2}\theta \\ \frac{l}{2}\theta \\ 1 \\ 1 \end{Bmatrix} \quad [68]$$

Because the system is now a rigid body, the coupled motion of the mode shape in equation 68 results in rotation of the twin-building system about the centroid location between the two buildings. This mode shape has downward translational motion for building B1, upward translational motion for building B2, and counterclockwise rotation for each building. Thus resulting in coupled motion of the twin-building system about the centroid of the two building system.

Numerical analysis of the symbolic eigenvalue and eigenvector solutions determined from equation 53 are evaluated to determine if these results identify the same findings for the eigenvectors shown in equations 67 and 68.

3.3 Development of Risa-3D v9.0.1 Structural Analysis Model

Risa-3D Demonstration Version 9.0.1 structural engineering analysis software is used to create a representative model of the twin tall buildings connected by a skybridge to compare the software's results with those of the symbolic equations developed within this thesis. Risa-3D v9.0.1 allows the user to perform dynamic analysis of the structural model by placing representative masses at nodal points, assigning end fixities for

members, defining member geometry and material properties, as well as specifying joint boundary conditions to model linear or torsional springs at each nodal point.

Numerical values were input into the Risa-3D v9.0.1 model to perform analysis. Using Lim (2008) quantities as a basis, similar values are used for creation of the Risa-3D model. The cross-section of each building was assigned lengths of 40 m x 40 m ($D \times D$), the height set at 300 m (H), the skybridge elevation at 150 m ($h = H/2$), a spacing of 80 m (l) between the buildings' geometric centers, and a building gross mass density of 200 kg/m³ (ρ_m). The polar radius of gyration was assumed as $r_o = 0.3 D$. The natural frequencies of the uncoupled three modes assumed for each of the buildings not connected by the skybridge were: 0.16 Hz for the two translational (x and y) modes and 0.24 Hz for the torsional mode (θ) (Lim, 2008). From these quantities, masses and spring stiffnesses were assigned to the Risa-3D model.

A simple model was developed in Risa-3D v9.0.1. Figure 8 shows a plan view of the model created in Risa-3D that is representative of the views displayed in Figure 4 and Figure 5 for the twin tall buildings at the skybridge level. Figure 8 only shows the nodal points and the centerline of the skybridge members. Nodes are shown in Figure 8 and represented by an N followed by the number of the corresponding node. Node $N4$ on the left hand side of Figure 8 and node $N2$ on the right hand side represent the geometric centers of buildings B1 and B2 respectively. Nodes $N6$ and $N5$ represent the ends of the rigid links present at each end of the skybridge as depicted in Figure 5. There are three different members that make up the skybridge model shown in Figure 8. Member $M3$ shown in the middle represents the portion of the skybridge that has properties of EA and EI that are varied to analyze the response of the buildings due to the changing of these

properties. Members $M5$ and $M4$ represent the rigid end links that may or may not exist at the ends of the skybridge. It should be noted that members $M5$ and $M4$ were removed and only member $M3$ was used to represent the scenario where the length of the rigid end section parameter $b = 0$. Likewise, the properties of members $M5$ and $M4$ are assigned properties so these members have a stiffness ratio infinitely large in relation to member $M3$. The coordinates of nodes $N6$ and $N5$ are changed to vary the length of the rigid end sections of length b displayed in Figure 5. Solid square cross sectional shapes were assigned to all three members of Figure 8. The area A and moment of inertia I were fixed for all cases of analysis and the modulus of elasticity E was varied to provide the differences in the values of ψ_B that were targeted.

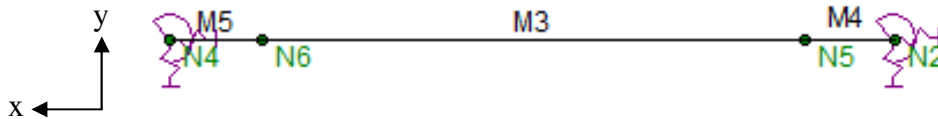


Figure 8. Risa-3D v9.0.1 Structural Analysis Model Plan View

It cannot be shown in Figure 8, but as mentioned earlier, lumped masses are placed at nodes $N4$ and $N2$ representing the masses of each building. For this model, the masses were determined from the properties listed in this section and calculated using equations 21 and 22. These masses were designated for the x -, y - and θ -directions.

Also shown in Figure 8 are the boundary conditions assigned for nodes $N4$ and $N2$. It can be seen that linear springs are shown in Figure 8 for the x - and y -directions. Also, a torsional spring is assigned at these two nodes as well. The equivalent spring forces assigned for each boundary condition were calculated from equation 23 for the linear springs and equation 24 for the torsional spring as based on the properties outlined in this section.

Figure 9 shows an isometric view of the model created in Risa-3D v9.0.1. As can be seen, the vertical support of the model is handled by two short, massless members $M1$ and $M2$ with zero stiffness. Nodes $N1$ and $N3$ were designed with a pinned connection as shown to allow free rotation about any direction. Stability of the model in the x - and y -directions is provided by the linear springs discussed earlier. The two massless members $M1$ and $M2$ were used because Risa-3D would not analyze the model with vertical support being placed directly at nodes $N2$ and $N4$.

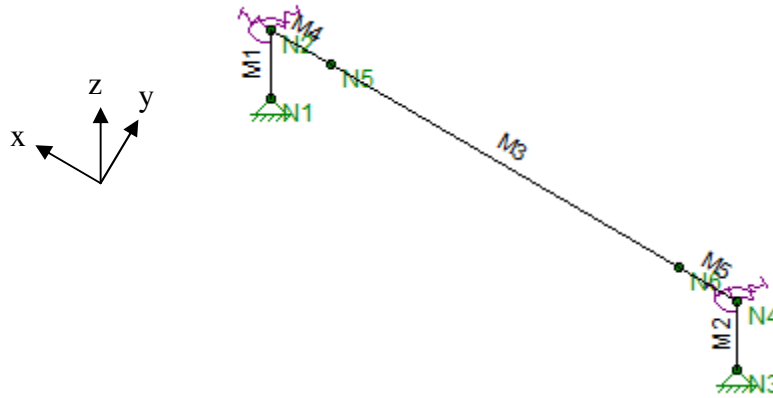


Figure 9. Isometric view of Risa-3D v9.0.1 structural analysis model.

Table 1 through Table 5 show specific properties entered into Risa-3D v9.0.1 for the model where the rigid end link has a length of $b = 10\text{ m}$ and the skybridge modulus of elasticity a value of $E = 20,000\text{ MPa}$. Similar properties were used for analysis of the other models where $b = 0\text{ m}$ and 20 m and $E = 5,000\text{ MPa}$ and $10,000\text{ MPa}$.

Table 1. Risa-3D v9.0.1 Member Primary Data for $b = 10\text{ m}$ and $E = 20000\text{ MPa}$

Label	I Joint	J Joint	Section/Shape	Type	Design List	Material
M1	N1	N2	Building	Column	None	Massless
M2	N3	N4	Building	Column	None	Massless
M3	N5	N6	Bridge	Beam	None	Bridge
M4	N2	N5	Bridge_Infinite	Beam	None	Bridge_Infinite
M5	N6	N4	Bridge_Infinite	Beam	None	Bridge_Infinite

Table 2. Risa-3D v9.0.1 General Material Properties for $b = 10\text{ m}$ and $E = 20000\text{ MPa}$

Label	E [MPa]	G [MPa]	Nu	Therm (/1E5 C)	Density (kg/m ³)
Building	1.00E-06	0	0.3	0	0
Bridge	20000	1923.077	0.3	1.17	0
Bridge_Infinite	1.00E+07	3.00E+06	0.3	1.17	0

Table 3. Risa-3D v9.0.1 Joint Coordinates for $b = 10\text{ m}$ and $E = 20000\text{ MPa}$

Label	X [m]	Z [m]	Y [m]
N1	0	140	0
N2	0	150	0
N3	80	140	0
N4	80	150	0
N5	10	150	0
N6	70	150	0

Table 4. Risa-3D v9.0.1 Joint Boundary Conditions for $b = 10\text{ m}$ and $E = 20000\text{ MPa}$

Joint Label	X [kN/mm]	Z [kN/mm]	Y [kN/mm]	X Rot. [kN-m/rad]	Z Rot. [kN-m/rad]	Y Rot. [kN-m/rad]
N1	Reaction	Reaction	Reaction	-	-	-
N3	Reaction	Reaction	Reaction	-	-	-
N2	S129.363	-	S129.363	-	S2.096e+7	-
N4	S129.363	-	S129.363	-	S2.096e+7	-

Table 5. Risa-3D v9.0.1 Joint Loads and Enforced Displacements for $b = 10\text{ m}$ and $E = 20000\text{ MPa}$

Joint Label	L,D,M	Direction	Magnitude [(kN,kN-m), (mm,rad), (kN*s ² /m, kN*m ²)]
N2	M	X	1.28E+05
N4	M	X	1.28E+05
N2	M	MZ	9.22E+06
N4	M	MZ	9.22E+06
N2	M	Y	1.28E+05
N4	M	Y	1.28E+05

4. Results and Discussion

4.1 Results from Symbolic Computing

4.1.1 Eigenvalue Results

Analysis of the two symbolic matrices outlined in equations 38 and 53 for the x -direction and y - θ directions respectively with the symbolic computing software Maple 13 yields the resulting six eigenvalue solutions:

$$\lambda_{x,in} = 1 \quad [69]$$

$$\lambda_{x,out} = 1 + 2\psi_A \quad [70]$$

$$\lambda_{y,in} = 1 \quad [71]$$

$$\lambda_{y,out} = \frac{1}{2}(1 + \kappa) + \psi_B \left(1 + \frac{l^2}{4r_0^2}\right) - \frac{1}{2}\sqrt{\mu} \quad [72]$$

$$\lambda_{\theta,in} = \left(\frac{1}{2}(1 + \kappa) + \psi_B \left(1 + \frac{l^2}{4r_0^2}\right) + \frac{1}{2}\sqrt{\mu}\right) \quad [73]$$

$$\lambda_{\theta,out} = \left(\kappa + \frac{2EI}{k_y^e r_0^2 l}\right) \quad [74]$$

where

$$\mu = \kappa^2 - 2\kappa + \psi_B \kappa \left(\frac{l^2}{r_0^2} - 4\right) + \left(-\psi_B \left(\frac{l^2}{2r_0^2} - 2\right) + 1\right)^2 + 4\psi_B^2 \frac{l^2}{r_0^2} \quad [75]$$

The formulas in equations 69 and 70 show the eigenvalues associated with the equations of motion for the x -direction. Similarly, equations 71 through 74 display the eigenvalues for the y - θ equations of motion. As seen in equations 69 through 74, there are two eigenvalues associated with each of the three principal directions of the twin tall building model. They are denoted as “in” and “out” which is associated with in-phase movement and 180 degrees out-of-phase movement. The complete un-simplified expressions

corresponding to equations 71 through 74 for the y - and θ -directions as output by Maple 13 are displayed in Appendix D.

Recall from Section 3.1 that the final form of the matrix in equation 38 associated with the x -direction specified $m_x^e \omega^2 / k_x^e = \lambda$, therefore the final resulting normalized natural frequencies for the x -direction are expressed by taking the square root of the previous formulas:

$$\Omega_{x,in} = 1 \quad [76]$$

$$\Omega_{x,out} = \sqrt{1 + 2\psi_A} \quad [77]$$

Likewise, the symbolic results of equation 53 associated with the y -direction specified $m_y^e \omega^2 / k_y^e = \lambda$, the resulting final normalized natural frequencies are:

$$\Omega_{y,in} = 1 \quad [78]$$

$$\Omega_{y,out} = \left(\frac{1}{2}(1 + \kappa) + \psi_B \left(1 + \frac{l^2}{4r_0^2} \right) - \frac{1}{2}\sqrt{\mu} \right)^{1/2} \quad [79]$$

The eigenvalue results for the two modes in the θ -direction require one additional step to determine the normalized natural frequency. Similar to modes in the y -direction, $m_y^e \omega^2 / k_y^e = \lambda$ was specified. However, it is desired that the two modes associated with the θ -direction be normalized to the torsional natural frequency. Therefore, each mode for the θ -direction is multiplied by $1/\kappa$ and the square root taken which results in the final normalized natural frequencies:

$$\Omega_{\theta,in} = \left[\left(\frac{1}{2}(1 + \kappa) + \psi_B \left(1 + \frac{l^2}{4r_0^2} \right) + \frac{1}{2}\sqrt{\mu} \right) \frac{H \omega_y^2}{h \omega_\theta^2} \right]^{1/2} \quad [80]$$

$$\Omega_{\theta,out} = \left[\left(\kappa + \frac{2EI}{k_y^e r_0^2 l} \right) \frac{H \omega_y^2}{h \omega_\theta^2} \right]^{1/2} \quad [81]$$

4.1.2 Mode Shapes of y - θ motion

In addition to the determination of the eigenvalues of equations 38 and 53, Maple 13 was used to symbolically determine the modal shapes corresponding to the six eigenvalues. Determination of the mode shapes are as follows:

$$\{\phi\}_{x,in} = \begin{Bmatrix} 1 \\ 1 \end{Bmatrix} \quad [82]$$

$$\{\phi\}_{x,out} = \begin{Bmatrix} 1 \\ -1 \end{Bmatrix} \quad [83]$$

$$\{\phi\}_{y,in} = \begin{Bmatrix} 1 \\ 0 \\ 0 \end{Bmatrix} \quad [84]$$

$$\{\phi\}_{y,out} = \begin{Bmatrix} 1 \\ -1 \\ -\left(\frac{1}{r_N}\right)_{y,out} \\ -\left(\frac{1}{r_N}\right)_{y,out} \end{Bmatrix} \quad [85]$$

$$\{\phi\}_{\theta,in} = \begin{Bmatrix} (r_N)_{\theta,in} \\ -(r_N)_{\theta,in} \\ 1 \\ 1 \end{Bmatrix} \quad [86]$$

$$\{\phi\}_{\theta,out} = \begin{Bmatrix} 0 \\ 0 \\ 1 \\ -1 \end{Bmatrix} \quad [87]$$

where

$$\left(\frac{1}{r_N}\right)_{y,out} = \frac{\left[\left(\left(\frac{\sqrt{\mu}}{2\psi_B} - 1 \right) - \frac{l^4}{4r_0^2} + (1 + \sqrt{\mu} + 2\psi_B) \frac{r_0^2}{l^2\psi_B^2} \right) 4l^2 r_0^2 \psi_B^2 (k_y^e)^2 + (-2 - \sqrt{\mu} - 2\psi_B) 4k_\theta^e r_0^2 k_y^e + 4(k_\theta^e)^2 \right]}{4\psi_B l k_y^e r_0 \left(\left((-2\psi_B - 3 + \sqrt{\mu})r_0^2 - \frac{\psi_B l^2}{2} \right) k_y^e + 3k_\theta^e \right)} \quad [88]$$

$$(r_N)_{\theta,in} = \frac{4\psi_B l k_y^e r_0 \left(\left((2\psi_B + 3 + \sqrt{\mu})r_0^2 + \frac{\psi_B l^2}{2} \right) k_y^e - 3k_\theta^e \right)}{\left[\left(\left(\frac{\sqrt{\mu}}{2\psi_B} + 1 \right) + \frac{l^4}{4r_0^2} + (-1 + \sqrt{\mu} - 2\psi_B) \frac{r_0^2}{l^2\psi_B^2} \right) 4l^2 r_0^2 \psi_B^2 (k_y^e)^2 + (2 - \sqrt{\mu} + 2\psi_B) 4k_\theta^e r_0^2 k_y^e - 4(k_\theta^e)^2 \right]} \quad [89]$$

where r_N is the effective radius of rotation.

The effective radius of rotation describes the coupled motion of the translational and rotational components of mode shapes y -out and θ -in. The effective radius of rotation is non-dimensional and expressed as:

$$r_N = \frac{u_y^e h}{u_\theta^e H r_0} \quad [90]$$

As seen in equations 85 and 86, modes y -out and θ -in possess a primary component and a secondary component resulting in coupled motion. For mode y -out, there is a primary translational component and a secondary rotational component represented by equation 88. Similarly, mode θ -in has a primary rotational component and a secondary translational component represented by equation 89. Conversely, equations 82 through 84 and 87 show the modal shapes for modes x -in, x -out, y -in and θ -out to be purely translational or purely rotational. Figure 10 graphically shows the six mode shapes as determined from the symbolic analysis of the twin tall building system and displays these modes grouped by the principal direction of the dominant building motion. Figure 10 (a) shows the motion relating to the x -direction. As shown in the figure, mode x -in displays the two buildings moving in the same directions. Conversely, mode x -out displays the two buildings moving in opposite directions. The same trend is displayed in Figure 10 (b) and Figure 10 (c) with the addition of the coupled movement for mode y -out and θ -in.

The two expressions for equations 88 and 89 are simplified from their full form by the elimination of terms having no influence on the formulas within the expected design range of ψ_B . The range of ψ_B specified is from 0 to 1.5 with the upper limit being beyond the expected value for the relative bending stiffness ψ_B . An additional simplification is made from the final output of Maple 13 to the final form of the equations

in 88 and 89. The final results from Maple 13 show individual expressions for the third and fourth terms of the vector in equation 85 and the first and second terms of the vector in equation 86. However, numerical analysis of these equations yield the same values

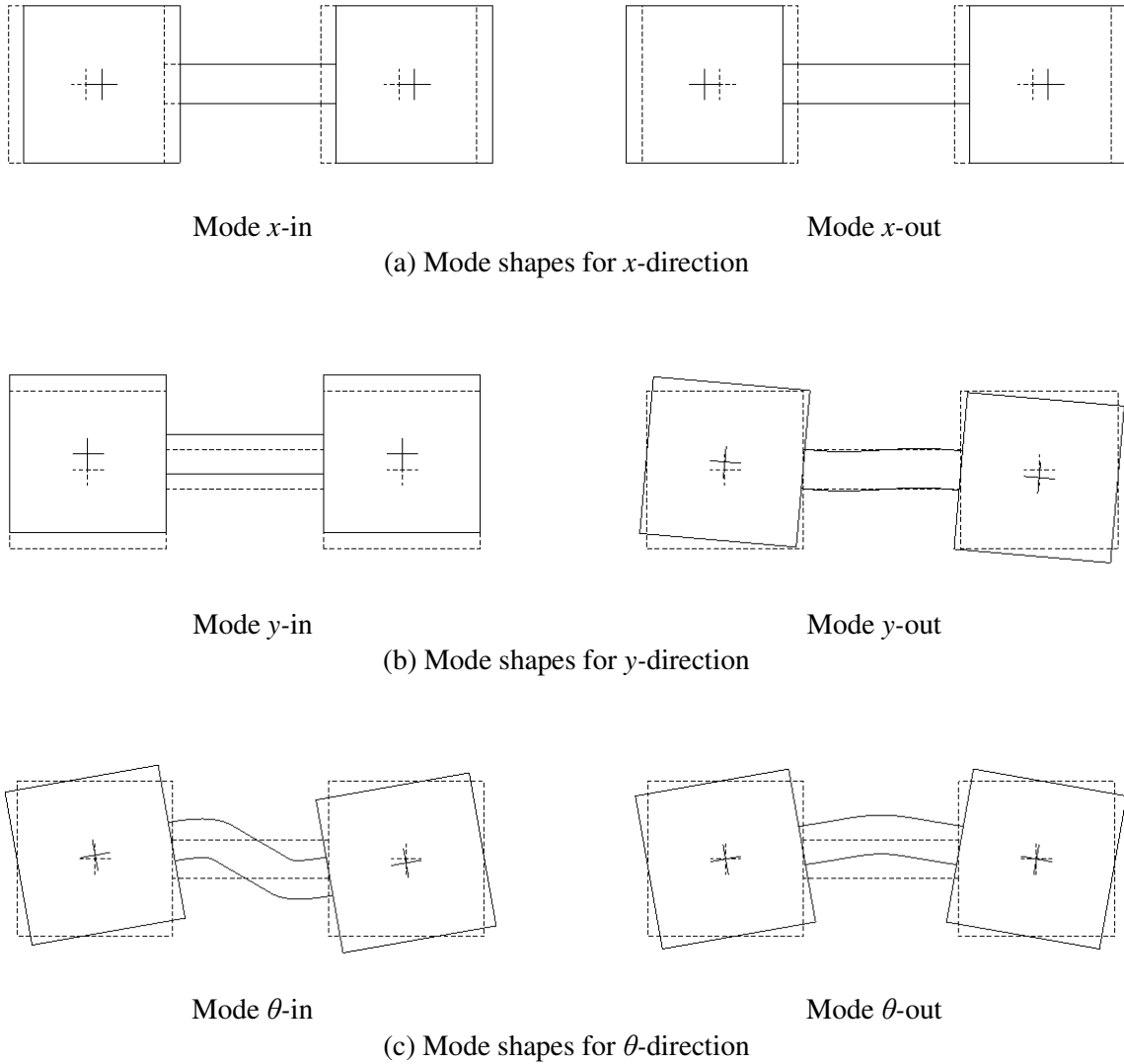


Figure 10. Mode shapes for six natural modes determined for twin-tall buildings connected by a skybridge.

within the range of ψ_B mentioned previously and were therefore reduced to a single expression for each of the respective mode shapes, y -out and θ -in. The following formulas are the final symbolic output for the coupled mode shapes from Maple 13 that

were simplified to the effective radius of rotation expressions shown in equations 88 and 89.

$$\{\phi\}_{y,out} = \begin{pmatrix} \frac{-y_1}{\theta_1} \\ y_2 \\ \theta_2 \\ 1 \\ 1 \end{pmatrix} \quad [91]$$

where

$$\frac{-y_1}{\theta_1} = \frac{2\psi_B\alpha_1 \left(\left(\psi_B + \frac{1}{2}\kappa + \frac{1}{2}\psi_B\alpha_3 + \frac{1}{2} + \frac{1}{2}\psi_B\alpha_2 - \frac{1}{2}\sqrt{\mu} \right) (\kappa - \psi_B - 4\psi_B\alpha_1^2 + \psi_B\alpha_2 + \psi_B\alpha_3) - \frac{3}{2} \left(\kappa + \psi_B\alpha_3 + \psi_B\alpha_2 - \frac{8}{3}\psi_B\alpha_1^2 \right) + \frac{1}{2} + \frac{1}{2}\sqrt{\mu} \right)}{\left[\left(\left(\psi_B + \frac{1}{2}\kappa + \frac{1}{2}\psi_B\alpha_3 + \frac{1}{2} + \frac{1}{2}\psi_B\alpha_2 - \frac{1}{2}\sqrt{\mu} \right) (\kappa - 4\psi_B\alpha_1^2 + \psi_B\alpha_2 + \psi_B\alpha_3) + \psi_B + \frac{1}{2} \right) - \frac{3}{2} \left(\kappa + \psi_B\alpha_2 + \psi_B\alpha_3 \right) + \frac{1}{2}\sqrt{\mu} + 4\psi_B\alpha_1^2 - 2\psi_B^2\alpha_2 - 2\kappa\psi_B + 4\psi_B^2\alpha_1^2 - 2\psi_B^2\alpha_3 \right] \times \frac{1}{2} (\kappa + \psi_B\alpha_3 - 1 + \psi_B\alpha_2 - \sqrt{\mu})} \quad [92]$$

$$\frac{y_2}{\theta_2} = \frac{2\psi_B\alpha_1 \left(-\frac{3}{2}\psi_B\alpha_2 - \frac{3}{2}\kappa + 4\psi_B^2\alpha_1^2 - \frac{3}{2}\psi_B\alpha_3 + \frac{3}{2} + \psi_B - \frac{1}{2}\sqrt{\mu} \right)}{\left(\left(\psi_B + \frac{1}{2}\kappa + \frac{1}{2}\psi_B\alpha_3 + \frac{1}{2} + \frac{1}{2}\psi_B\alpha_2 - \frac{1}{2}\sqrt{\mu} \right) (\kappa - 4\psi_B\alpha_1^2 + \psi_B\alpha_2 + \psi_B\alpha_3) + \psi_B + \frac{1}{2} \right) - \frac{3}{2} \left(\kappa + \psi_B\alpha_2 + \psi_B\alpha_3 \right) + \frac{1}{2}\sqrt{\mu} + 4\psi_B\alpha_1^2 - 2\psi_B^2\alpha_2 - 2\kappa\psi_B + 4\psi_B^2\alpha_1^2 - 2\psi_B^2\alpha_3} \quad [93]$$

For

$$\{\phi\}_{\theta,in} = \begin{pmatrix} \frac{y_1}{\theta_1} \\ -y_2 \\ \theta_2 \\ 1 \\ 1 \end{pmatrix} \quad [94]$$

where

$$\frac{y_1}{\theta_1} = \frac{2\psi_B\alpha_1 \left((\psi_B(-1 + \alpha_2 + \alpha_3 - 4\alpha_1^2) + \kappa) \left(\frac{1}{2}(2\psi_B + \kappa + \psi_B\alpha_3 + 1 + \psi_B\alpha_2 + \sqrt{\mu}) \right) - \frac{3}{2} \left(\kappa + \psi_B\alpha_3 + \psi_B\alpha_2 - \frac{8}{3}\psi_B\alpha_1^2 \right) + \frac{1}{2}(1 - \sqrt{\mu}) \right)}{\left[\left(\frac{1}{2}(2\psi_B + \kappa + \psi_B\alpha_3 + 1 + \psi_B\alpha_2 + \sqrt{\mu})(\psi_B\alpha_2 + \kappa - 4\psi_B\alpha_1^2 + \psi_B\alpha_3) - \frac{3}{2} \left(\kappa + \psi_B\alpha_3 + \psi_B\alpha_2 - \frac{8}{3}\psi_B\alpha_1^2 \right) + 2 \left(\frac{1}{2}\psi_B + \frac{1}{4} - \frac{1}{4}\sqrt{\mu} - \psi_B^2\alpha_2 - \kappa\psi_B + 2\psi_B^2\alpha_1^2 - \psi_B^2\alpha_3 \right) \right) \times \left(\frac{1}{2}(\kappa + \psi_B\alpha_3 - 1 + \psi_B\alpha_2 + \sqrt{\mu}) \right) \right]} \quad [95]$$

$$\frac{-y_2}{\theta_2} =$$

$$\frac{2\psi_B\alpha_1 \left(-\frac{3}{2}\psi_B\alpha_2 - \frac{3}{2}\kappa + 4\psi_B^2\alpha_1^2 - \frac{3}{2}\psi_B\alpha_3 + \frac{3}{2} + \psi_B + \frac{1}{2}\sqrt{\mu} \right)}{\left(\left(\psi_B + \frac{1}{2}\kappa + \frac{1}{2}\psi_B\alpha_3 + \frac{1}{2} + \frac{1}{2}\psi_B\alpha_2 + \frac{1}{2}\sqrt{\mu} \right) (\kappa - 4\psi_B\alpha_1^2 + \psi_B\alpha_2 + \psi_B\alpha_3) + \psi_B + \frac{1}{2} \right) - \frac{3}{2}(\kappa + \psi_B\alpha_2 + \psi_B\alpha_3) - \frac{1}{2}\sqrt{\mu} + 4\psi_B\alpha_1^2 - 2\psi_B^2\alpha_2 - 2\kappa\psi_B + 4\psi_B^2\alpha_1^2 - 2\psi_B^2\alpha_3} \quad [96]$$

As mentioned in Section 1.3.1 and illustrated in equations 92 and 93 as well as 95 and 96, the final formulas can be long and cumbersome and take considerable effort by the user to reduce to a workable format.

Additional modal shape analysis was performed on the coupled motion of modes y -out and θ -in and their effective radius of rotation values. Figure 11 (a) and (b) show the motion of the coupled modes y -out and θ -in respectively. Figure 11 (c) shows parametrically how the value of r_N changes as ψ_B is increased for the particular situation of $b = 0 \text{ m}$. The trends are similar for $b = 10 \text{ m}$ and $b = 20 \text{ m}$. As seen in Figure 11 (c) and illustrated in Figure 11 (a), as the value of ψ_B decreases, the effective radius of rotation increases for mode y -out. Thus viewed in Figure 11 (a), as the value of ψ_B goes to zero, the effective radius of rotation goes to infinity and mode y -out shows purely translational motion in lieu of the coupled translational-rotational motion at larger values of ψ_B . Similarly, mode θ -in shown in Figure 11 (b) and (c) show as the value of ψ_B decreases, the effective radius of rotation tends to zero. Thus viewed in Figure 11 (b), as

ψ_B decreases, r_N decreases until mode θ -in is purely rotational and no longer displays coupled rotational-translational motion. As the relative bending stiffness ψ_B decreases and approaches zero, the buildings display behavior of unconnected buildings. These trends and diagrams match the findings in Lim (2008).

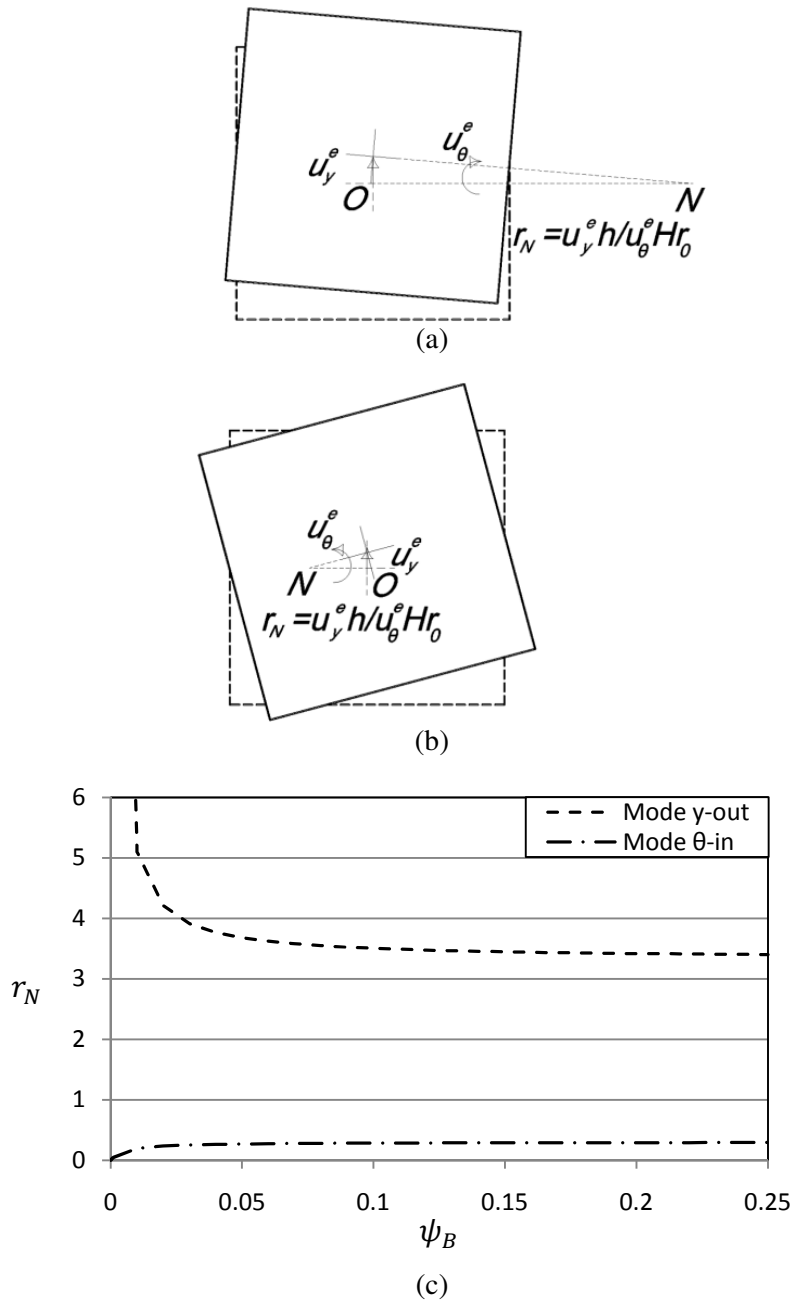


Figure 11. (a) Schematic showing effective radius of rotation for mode y-out; (b) Schematic showing effective radius of rotation for mode θ -in; (c) Comparison of effective radius of rotation values for coupled mode y-out and θ -in.

4.1.3 Uncoupling of y - θ motion

If the value of $\psi_B = 0$, then the (4 x 4) matrix of equation 53 becomes diagonal and the cross-coupling between the y - and θ -directions does not exist. When this occurs, the equations of motion in the y - and θ -directions can be treated as four independent equations and the motions in the y - and θ -directions can be analyzed independently.

The off-diagonal (2 x 2) block matrix values in equation 53 were examined to determine their significance in the calculated natural frequencies and modal shapes. If these terms were very small, they could be neglected and this approximation would lead to two (independent) 2DOF systems and a simplified analytical solution (similar to that for the x -direction) could be obtained. However, it was found that the off-diagonal (2 x 2) terms of equation 53 were not insignificant in presence of the coupling relative bending stiffness ψ_B . As a result, the coupled (4 x 4) matrix equations had to be employed to determine the natural frequencies and modal shapes. These quantities were obtained symbolically as outlined in Section 4.1.

4.2 Numerical Results of Symbolic Equations for 4 Degrees-of-Freedom Reduced to 2 Degrees-of-Freedom

Using the building properties outlined in Section 3.3, the symbolic expressions shown in equations 78 through 81 for the normalized natural frequencies for y - and θ -modes and the modal shapes in equations 84 through 87 and the effective radius values in equations 88 and 89 were evaluated numerically. The results were analyzed to determine if the equations characterize the behavior of the building system as parameter b approaches $l/2$ and the system transforms from 4DOF to 2DOF.

Two methods were used to analyze the numeric results of the symbolic expressions and evaluate their behavior as parameter b approaches $l/2$. Maple 13 and Microsoft Excel were used for the numeric evaluation of the formulas. In both instances, it was found that the normalized natural frequency values for equations 79 and 81, or modes y -out and θ -out respectively, equal zero once parameter b equals a value of $1.0 \times 10^{-9} < l/2$. From this finding, it is determined that the symbolic formulas do model the building system reduction from 4DOF to 2DOF. This is observed in both the Maple 13 and Microsoft Excel examples. Table 6 shows the results of the Maple 13 and Microsoft Excel worksheets. From Table 6, it can be viewed that the normalized natural frequency value Ω for mode θ -in becomes very large and thus the system becomes infinitely rigid.

Table 6. Normalized natural frequency values for y and θ modes with $b = 1.0 \times 10^{-9} < l/2$ from Maple 13 and Microsoft Excel.

EI Values (kN-m ²)	Stiffness Ratio Values	Mode	Symbolic Values Ω
$EI = 1.04 + E09$	$\psi_B = 1.2 + E28$	y-in	1.000
		θ -out	0.000
		θ -in	$5.099 + E14$
		y-out	0.000

From the findings of the normalized natural frequency values in Table 6, it is determined that since modes y -out and θ -out are zero, their respective mode shapes shut off and are no longer present. Modes y -in and θ -in remain as the only two modes present and thus the system is reduced to 2DOF. Since only two modes shapes are now present, their corresponding modal shapes as determined from evaluation of equations 84 and 86 by Maple 13 and Microsoft Excel are as follows:

$$\{\phi\}_{y,in} = \begin{pmatrix} 1 \\ 1 \\ 0 \\ 0 \end{pmatrix} \quad [97]$$

$$\{\phi\}_{\theta,in} = \begin{pmatrix} -0.3 \\ 0.3 \\ 1 \\ 1 \end{pmatrix} \quad [98]$$

The results in equations 97 and 98 show the numerical values obtained match the expected mode shape shown in equations 67 and 68.

The ability of the symbolic expressions developed in this thesis are shown to model the behavior of the building system as the skybridge becomes infinitely rigid and thusly transforms to a 2DOF system from a 4DOF system. The results show the symbolic formulas model the behavior of the building system for the normalized natural frequencies and modal shapes as the parameter b approached the limit of $l/2$ and rigid body motion. Table 6 shows that as parameter b approaches a value approximately equal to $l/2$, mode y -out and θ -out equal zero and are no longer present.

4.3 Risa-3D Model Results

4.3.1 Comparison of Modal Natural Frequencies

Comparisons of the frequency values determined by the symbolic formulas derived in this thesis are compared to the Risa-3D v9.0.1 model results using the parameters defined in Section 3.3. In comparing the values, a difference of less than 0.2% was found between the frequencies for modes x -in, x -out, y -in and θ -out shown in equations 76 through 78 and 81 and those of the Risa-3D v9.0.1 model for all variations of parameter b and E . Due to the small difference between these values, only the frequencies of modes y -out and θ -in are discussed further. Three different values for parameter b ($b = 0 \text{ m}, 10 \text{ m}, 20 \text{ m}$) were used to compare the frequency values between

the equations of this thesis and those of the Risa-3D v9.0.1 model. Table 7 corresponds to $b = 0 \text{ m}$, Table 8 to $b = 10 \text{ m}$ and Table 9 to $b = 20 \text{ m}$. For each of these three values of parameter b , the value of E for the skybridge is varied to evaluate the difference of the frequencies between the symbolic formulas of this thesis and the Risa-3D model. As expected, the general trend for all three tables is as E decreases in value so do the frequencies. Likewise, as the value for parameter b increases and the effective length of the bridge ($l - 2b$) decreases, the frequency values increase as the value of ψ_B increases.

The comparison of the frequency values of the symbolic equations and the Risa-3D v9.0.1 results for mode θ -in show good correlation. The largest difference between the values for $b = 0 \text{ m}$ is 3.625% and the difference decreases as the value of E decreases. The same can be said for $b = 10 \text{ m}$ and 20 m with the largest percent difference being 5.5% and 10.0% respectively. Similarly with these values, as E decreases, the percent difference between the values decrease.

As for mode y -out, the comparison of the frequencies between the symbolic formulas and results from Risa-3D v9.0.1 show stronger correlation with less than 2.0% difference for all situations. It should be noted there was less than 0.00007 Hz variation between any of the mode y -out frequencies for all values of parameter b and E . The effect on mode y -out frequencies due to coupling of the tall buildings is minimal and is illustrated in the small differences between the frequencies shown in Table 7, Table 8 and Table 9. Regardless, the symbolic equations are closely correlated for this particular mode with the Risa-3D v9.0.1 results.

Table 7. Comparison of frequency results of modes θ -in and y -out for parameter $b = 0$ m and varying E of the skybridge for thesis equations vs. Risa-3D model.

E Values (MPa)	Stiffness Ratio Values	Mode	Symbolic Values f (Hz)	Risa-3D Values f (Hz)	% Diff
$E = 20000$	$\psi_B = 0.2$	θ -in	0.53956	0.52000	3.625%
		y -out	0.16080	0.16400	1.988%
$E = 10000$	$\psi_B = 0.1$	θ -in	0.41727	0.40900	1.982%
		y -out	0.16078	0.16300	1.378%
$E = 5000$	$\psi_B = 0.05$	θ -in	0.34004	0.33500	1.483%
		y -out	0.16075	0.16300	1.401%

Table 8. Comparison of frequency results of modes θ -in and y -out for parameter $b = 10$ m and varying E of the skybridge for thesis equations vs. Risa-3D model.

E Values (MPa)	Stiffness Ratio Values	Mode	Symbolic Values f (Hz)	Risa-3D Values f (Hz)	% Diff
$E = 20000$	$\psi_B = 0.4$	θ -in	0.78220	0.73900	5.523%
		y -out	0.16081	0.16400	1.981%
$E = 10000$	$\psi_B = 0.2$	θ -in	0.57833	0.56100	2.996%
		y -out	0.16081	0.16400	1.986%
$E = 5000$	$\psi_B = 0.1$	θ -in	0.44247	0.43100	2.593%
		y -out	0.16079	0.16300	1.374%

Table 9. Comparison of frequency results of modes θ -in and y -out for parameter $b = 20$ m and varying E of the skybridge for thesis equations vs. Risa-3D model.

E Values (MPa)	Stiffness Ratio Values	Mode	Symbolic Values f (Hz)	Risa-3D Values f (Hz)	% Diff
$E = 20000$	$\psi_B = 1.5$	θ -in	1.38902	1.25000	10.009%
		y -out	0.16082	0.16400	1.977%
$E = 10000$	$\psi_B = 0.75$	θ -in	0.99661	0.95000	4.677%
		y -out	0.16082	0.16400	1.978%
$E = 5000$	$\psi_B = 0.38$	θ -in	0.72468	0.69200	4.509%
		y -out	0.16081	0.16400	1.982%

4.3.2 Comparison of Modal Shapes

Figure 10 shows the six modal shapes present in the coupled building system as determined by the symbolic analysis. Figure 10 (a) shows the sway modal shapes in the x -direction, Figure 10 (b) shows the sway modal shapes in the y -direction including the coupled modal shape y -out and Figure 10 (c) shows the torsional mode shapes about the z -axis including the coupled mode θ -in.

A comparison of the modal shapes as determined from the symbolic equations versus the Risa-3D v9.0.1 model was performed. The same mode shapes were found regarding the four un-coupled modes of the Risa-3D v9.0.1 model and the results of this thesis. A difference exists between the two coupled mode shape solutions. The difference exhibited is between the positive and negative signs as displayed by the symbolic solutions when compared to results of the Risa-3D v9.0.1 model. The symbolic solutions have a sign convention of $\{\phi\}_{y,out}^T = \{(+)\ (-)\ (-)\ (-)\}$ and $\{\phi\}_{\theta,in}^T = \{(+)\ (-)\ (+)\ (+)\}$ respectively whereas the results from the Risa-3D model have signs of $\{\phi\}_{y,out}^T = \{(+)\ (-)\ (+)\ (+)\}$ and $\{\phi\}_{\theta,in}^T = \{(-)\ (+)\ (+)\ (+)\}$ respectively. It is suspected that this difference exists because of differing algorithms available for determining eigenvectors. The mode shapes as determined from the Risa-3D v9.0.1 model are shown in Figure 12 for the particular case of $b = 10\ m$ and $E = 20,000\ MPa$. Similar mode shapes exist for the other two lengths of parameter b and values of E . The modes are shown grouped by principal direction of the corresponding mode shape, i.e. x -in and x -out, y -in and y -out, θ -in and θ -out. For clarity and due to difficulty in accurately displaying the rotation of the building sections in Risa-3D, the full un-deformed model including building, rigid end sections

and skybridge sections is depicted in Figure 12 (a), while Figure 12 (b) through (g) show only the rigid end sections and the skybridge portions of the model.

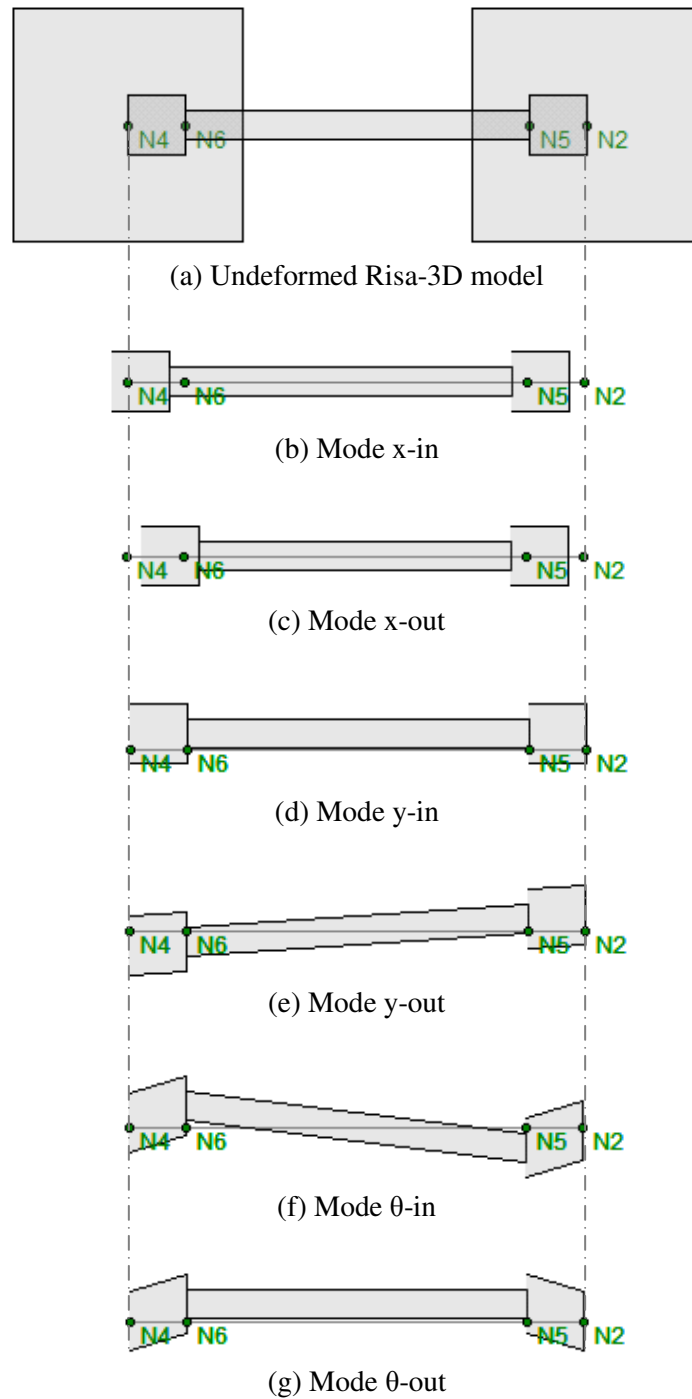


Figure 12. Risa-3D v9.0.1 modal shapes for $b=10\text{ m}$ and $E=20000\text{ MPa}$.

The modal shapes determined from the symbolic expressions developed in this thesis match those determined by Lim (2008). Comparison of the modal shapes differed however from those found in the Risa-3D v9.0.1 model for the two coupled modes y -out and θ -in. The differences can be viewed when examining Figure 10 and Figure 12. The two coupled modal shapes showed differences in signs for the translational components of mode y -out and the rotational components of θ -in. The remaining four mode shapes for this thesis and the Risa-3D results were in agreement.

5. Conclusions and Recommendation for Future Research

The connection of two twin tall towers by a skybridge has the potential to be a valuable tool for structural engineers to control vibrational motions. This research has demonstrated how the use of symbolic computing tools along with a simplified model of twin tall buildings with equivalent mass and stiffness reduced to the skybridge level can be used to determine the dynamic modal properties of the building system. Specific findings and outcomes of thesis include:

- Symbolic analysis provides a useful platform for free vibration analysis of structurally coupled tall buildings.
- Symbolic expressions model the behavior of building system as properties are tested at their limit.
- Obtained symbolic equations show good agreement with Risa-3D results.
- Developed symbolic equations are proposed as a tool for use in preliminary analysis of tall buildings connected by a skybridge.

Future research could include the development of damping properties of the skybridge between the twin tall buildings. Also, research can be done to extend the symbolic formulas to include the forcing terms on the right hand side of the equations of motion. Lastly, further efforts could be performed on the various connection configurations that exist between the skybridge and the buildings to account for forces induced by vibrational motion in the x -direction of the coupled building system.

Bibliography

- Asano, M., Yamano, Y., Yoshie, K., Koike, Y., Nakagawa, K., & Murata, T. (2003).
Development of Active-Damping Bridges and Its Application to Triple High-Rise
Buildings. *Japan Society of Mechanical Engineers International Journal , Series
C, 46 (3)*, 854-860.
- Baker, W. F. (2010, March). Engineering an Idea: The Realization of the Burj Khalifa.
Civil Engineering , pp. 44-47.
- Banerjee, J. R. (2004). Development of an Exact Dynamic Stiffness Matrix for Free
Vibration Analysis of a Twisted Timoshenko Beam. *Journal of Sound and
Vibration* , 270, 379-401.
- Beltzer, A. I. (1990). Engineering Analysis via Symbolic Computation - a Breakthrough.
Applied Mechanics Reviews , 43 (5), 119-127.
- Bharti, S. D., Dumne, S. M., & Shrimali, M. K. (2010). Seismic Response Analysis of
Adjacent Buildings Connected with MR Dampers. *Engineering Structures* , 1-12.
- Bhaskararao, A. V., & Jangid, R. S. (2006). Seismic Analysis of Structures Connected
with Friction Dampers. *Engineering Structures* , 28, 690-703.
- Boggs, D. W., & Hosoya, N. (2001). Wind-Tunnel Techniques to Address Structures
with Multiple Coupled Interactions. *Proceedings of the 2001 Structures Congress
& Exposition*, (pp. 1-6). Washington D.C.

- Carpinteri, A., Lacidogna, G., & Puzzi, S. (2010). A Global Approach for Three-Dimensional Analysis of Tall Buildings. *The Structural Design of Tall and Special Buildings* , 19, 518-536.
- Christenson, R. E., Spencer Jr., B. F., & Johnson, E. A. (2007). Semiactive Connected Control Method for Adjacent Multidegree-of-Freedom Buildings. *Journal of Engineering Mechanics* , 133 (3), 290-298.
- Christenson, R. E., Spencer Jr., B. F., Johnson, E. A., & Seto, K. (2006). Coupled Building Control Considering the Effects of Building/Connector Configuration. *Journal of Structural Engineering* , 132 (6), 853-863.
- Hashemi, S. M., & Adique, E. J. (2010). A Quasi-Exact Dynamic Finite Element for Free Vibration Analysis of Sandwich Beams. *Applied Composite Materials* , 17 (2), 259-269.
- Kim, J., Ryu, J., & Chung, L. (2006). Seismic Performance of Structures Connected by Viscoelastic Dampers. *Engineering Structures* , 28, 183-195.
- Lee, D.-G., Kim, H.-S., & Ko, H. (2010). Evaluation of Coupling-Control Effect of a Sky-Bridge for Adjacent Tall Buildings. *The Structural Design of Tall and Special Buildings* , 1-20.
- Lim, J. (2008). *Structural Coupling and Wind-Induced Response of Twin Tall Buildings with a Skybridge. Ph.D. dissertation, Colorado State University, United States -- Colorado*. Retrieved January 5, 2011, from Publication No. AAT 3346482
- Lim, J., & Bienkiewicz, B. (2007). Wind-Induced Response of Structurally Coupled Twin Tall Buildings. *Wind and Structures* , 10 (4), 383-398.

Maple. (n.d.). Retrieved January 25, 2011, from Maplesoft:

http://www.maplesoft.com/products/maple/compare/symbolic_computation.aspx#

Mathematica. (n.d.). Retrieved January 3, 2011, from Wolfram:

<http://www.wolfram.com/mathematica/>

Meriam, J. L., & Kraige, L. G. (2002). *Engineering Mechanics Dynamics Fifth Edition* (Vol. 2). New York City: John Wiley & Sons.

Nolan, J. F. (1953). *Analytical Differentiation on a Digital Computer*. Massachusetts Institute of Technology.

Noor, A. K., & Andersen, C. M. (1979). Computerized Symbolic Manipulation in Structural Mechanics - Progress and Potential. *Computers and Structures* , 10, 95-118.

Pavlovic, M. (2003). Symbolic Computation in Structural Engineering. *Computers and Structures* , 2122-2134.

Prokic, A. (2010, March). Effect of Bracing on Linear Free Vibration Characteristics of Thin-Walled Beams with Open Cross Section. *Journal of Engineering Mechanics* , 282-289.

Prokic, A. (2006). On Fivefold Coupled Vibrations of Timoshenko Thin-Walled Beams. *Engineering Structures* , 54-62.

Rofail, A., & Holmes, J. (2007). High Frequency Base Balance Methodology for Linked Tall Buildings. *12th International Conference on Wind Engineering*, (pp. 1-7). Cairns.

Schlichting, H. (1979). *Boundary-Layer Theory*. McGraw-Hill, Inc.

- Sebastian, W. M. (2010). Criteria for Uniqueness and Extreme of Moments in Continuous End Spans with Differential Settlement. *Engineering Structures* , 32, 1568-1576.
- Sepe, V., & Augusti, G. (2001). A "Deformable Section" Model for the Dynamics of Suspension Bridges. Part I: Model and Linear Response. *Wind and Structures* , 4 (1), 1-18.
- Sepe, V., Diaferio, M., & Augusti, G. (2003). A "Deformable Section" Model for the Dynamics of Suspension Bridges. Part II: Nonlinear Analysis and Large Amplitude Oscillations. *Wind and Structures* , 6 (6), 451-470.
- Symbolic Computation*. (2010, December 2). Retrieved January 25, 2011, from Wikipedia: http://en.wikipedia.org/wiki/Symbolic_computing
- Thomson, W. T., & Dahleh, M. D. (1998). *Theory of Vibration with Applications, 5th Edition*. Prentice Hall.
- Thornton, C. H., Hungspruke, U., & Joseph, L. M. (1997). Design of the Worlds' Tallest Buildings - Petronas Twin Towers at Kuala Lumpur City Centre. *The Structural Design of Tall Buildings* , 6, 245-262.
- Videla, L., Baloa, T., Griffiths, D. V., & Cerrolaza, M. (2007). Exact Integration of the Stiffness Matrix of an 8-Node Plane Elastic Finite Element by Symbolic Computation. *Numerical Methods for Partial Differential Equations* , 249-261.
- Zhu, H. P., Ge, D. D., & Huang, X. (2010). Optimum Connecting Dampers to Reduce the Seismic Responses of Parallel Structures. *Journal of Sound and Vibration* , 1-19.

Appendix A

Derivation of generalized mass and stiffness:

Following is a full derivation of the generalized masses and stiffnesses using formulas and notation as shown in Lim (2008):

$$m_s(z)\ddot{u}_s(z, t) + k_s(z)u_s(z, t) = p_s(z, t) \quad [\text{A-1}]$$

$$u_s(z, t) = \phi_s(z)q_s(t) \quad [\text{A-2}]$$

$$\phi_s(z) = \left(\frac{z}{H}\right)^{\beta_s} \quad [\text{A-3}]$$

$$\beta_s = \beta_x = \beta_y = \beta_\theta = 1 \quad [\text{A-4}]$$

$$u_s(h, t) = \left(\frac{h}{H}\right)^{\beta_s} q_s(t) \quad [\text{A-5}]$$

$$q_s(t) = u_s(h, t) \left(\frac{H}{h}\right)^{\beta_s} \quad [\text{A-6}]$$

$$u_s(z, t) = \phi_s(z) \left(\frac{H}{h}\right)^{\beta_s} u_s(h, t) \quad [\text{A-7}]$$

$$\phi_s(z) \left(\frac{H}{h}\right)^{\beta_s} [m_s(z)\ddot{u}_s(h, t) + k_s(z)u_s(h, t)] = p_s(z, t) \quad [\text{A-8}]$$

$$\int_0^H \phi_s(z) \left\{ \phi_s(z) \left(\frac{H}{h}\right)^{\beta_s} [m_s(z)\ddot{u}_s(h, t) + k_s(z)u_s(h, t)] = p_s(z, t) \right\} dz \quad [\text{A-9}]$$

$$\left[\int_0^H [\phi_s(z)]^2 dz \right] \left\{ \left(\frac{H}{h}\right)^{\beta_s} [m_s(z)\ddot{u}_s(h, t) + k_s(z)u_s(h, t)] \right\} = \int_0^H p_s(z, t) \phi_s(z) dz \quad [\text{A-10}]$$

$$\frac{H}{2\beta_s + 1} \left(\frac{H}{h}\right)^{\beta_s} [m_s(z)\ddot{u}_s(h, t) + k_s(z)u_s(h, t)] = \int_0^H p_s(z, t) \phi_s(z) dz = P_s^*(t) \quad [\text{A-11}]$$

$$\frac{H}{2\beta_s + 1} \left(\frac{H}{h}\right)^{\beta_s} m_s(z) [\ddot{u}_s(h, t) + \omega_s^2(z) u_s(h, t)] = P_s^*(t) \quad [\text{A-12}]$$

$$m_s^* = \frac{H}{2\beta_s + 1} m_s \quad [\text{A-13}]$$

$$m_s = \rho_m D^2 \text{ for } s = x, y \quad [\text{A-14}]$$

$$m_s = \rho_m D^2 r_0^2 \text{ for } s = \theta \quad [\text{A-15}]$$

$$m_s^* \left(\frac{H}{h}\right)^{\beta_s} [\ddot{u}_s(h, t) + \omega_s^2(z) u_s(h, t)] = P_s^*(t) \quad [\text{A-16}]$$

$$P_s^*(t) = \int_0^H \left(\frac{z}{H}\right)^{\beta_s} p_s(z, t) dz = \frac{1}{H^{\beta_s}} \int_0^H z^{\beta_s} p_s(z, t) dz = \frac{1}{H^{\beta_s}} \frac{z^{\beta_s+1}}{\beta_s + 1} p_s(z, t) \Big|_0^H \quad [\text{A-17}]$$

$$P_s^*(t) = \frac{\lambda_s}{H^{\gamma_s}} M_{\bar{s}}(t) \quad [\text{A-18}]$$

$$\lambda_s = \frac{H^{\beta_s+1}}{\beta_s + 1} \quad [\text{A-19}]$$

$$\gamma_x = \gamma_y = 1 \text{ and } \gamma_\theta = 0 \quad [\text{A-20}]$$

$$M_{\bar{x}}(t) = M_y(t) \quad [\text{A-21}]$$

$$M_{\bar{y}}(t) = M_x(t) \quad [\text{A-22}]$$

$$M_{\bar{\theta}}(t) = M_\theta(t) \quad [\text{A-23}]$$

$$m_s^* \left(\frac{H}{h}\right)^{\beta_s} [\ddot{u}_s(h, t) + \omega_s^2(z) u_s(h, t)] = P_s^*(t) \quad [\text{A-24}]$$

$$m_s^* \left(\frac{H}{h}\right)^{\beta_s} [\ddot{u}_s(h, t) + \omega_s^2(z) u_s(h, t)] = \frac{\lambda_s}{H^{\gamma_s}} M_{\bar{s}}(t) \quad [\text{A-25}]$$

$$m_s^* \left(\frac{H}{h}\right)^{\beta_s} \left(\frac{H}{h}\right)^{\gamma_s} [\ddot{u}_s(h, t) + \omega_s^2(z) u_s(h, t)] = \frac{\lambda_s}{h^{\gamma_s}} M_{\bar{s}}(t) \quad [\text{A-26}]$$

$$m_s^e \ddot{u}_s(h, t) + k_s^e u_s(h, t) = P_s^e(t) \quad [\text{A-27}]$$

$$m_s^e = m_s^* \left(\frac{H}{h}\right)^{\beta_s + \gamma_s} \quad [\text{A-28}]$$

$$k_s^e = m_s^e \omega_s^2 \quad [\text{A-29}]$$

$$P_s^e(t) = \frac{\lambda_s}{h^{\gamma_s}} M_s(t) \quad [\text{A-30}]$$

$$m_x = m_y = \rho_m D^2 \text{ and } m_\theta = \rho_m D^2 r_0^2 \quad [\text{A-31}]$$

$$m_y^e = m_y^* \left(\frac{H}{h}\right)^{\beta_y + \gamma_y} = \frac{\rho_m D^2 H}{2\beta_y + 1} \left(\frac{H}{h}\right)^{\beta_y + \gamma_y} \quad [\text{A-32}]$$

$$m_y^e = \frac{\rho_m D^2 H}{3} \left(\frac{H}{h}\right)^2 = \left[\frac{\rho_m D^2 H^3}{3} \right] \left(\frac{1}{h^2}\right) = \frac{J_B}{h^2} \quad [\text{A-33}]$$

$$m_\theta^e = m_\theta^* \left(\frac{H}{h}\right)^{\beta_\theta + \gamma_\theta} = \frac{\rho_m D^2 r_0^2 H}{2\beta_\theta + 1} \left(\frac{H}{h}\right)^{\beta_\theta + \gamma_\theta} \left(\frac{h}{H}\right) \left(\frac{H}{h}\right) \quad [\text{A-34}]$$

$$m_\theta^e = \frac{\rho_m D^2 H^3}{3} \left(\frac{1}{h^2}\right) \left(\frac{h}{H}\right) r_0^2 = m_y^e \left(\frac{h}{H}\right) r_0^2 \quad [\text{A-35}]$$

Appendix B

Formation of equations from free body diagram for y - and θ -motions:

Summation of forces in the y -direction for building B1:

$$-k_y^e u_{y1}^e - \frac{12EI}{l_e^3} (u_{y1}^e - u_{y2}^e) - \frac{6EI}{l_e^2} (u_{\theta1}^e + u_{\theta2}^e) - \frac{12EI}{l_e^3} b (u_{\theta1}^e + u_{\theta2}^e) = m_y^e \ddot{y}_1 \quad [\text{B-1}]$$

Summation of forces in the y -direction for building B2:

$$-k_y^e u_{y2}^e + \frac{12EI}{l_e^3} (u_{y1}^e - u_{y2}^e) + \frac{6EI}{l_e^2} (u_{\theta1}^e + u_{\theta2}^e) + \frac{12EI}{l_e^3} b (u_{\theta1}^e + u_{\theta2}^e) = m_y^e \ddot{y}_2 \quad [\text{B-2}]$$

Summation of moments for building B1:

$$\begin{aligned} -k_\theta^e u_{\theta1}^e - \frac{6EI}{l_e^2} (u_{y1}^e - u_{y2}^e) - \frac{4EI}{l_e} u_{\theta1}^e - \frac{2EI}{l_e} u_{\theta2}^e - \frac{6EI}{l_e^2} b (u_{\theta1}^e + u_{\theta2}^e) \\ - \frac{12EI}{l_e^3} b (u_{y1}^e - u_{y2}^e) - \frac{6EI}{l_e^2} b (u_{\theta1}^e + u_{\theta2}^e) - \frac{12EI}{l_e^3} b^2 (u_{\theta1}^e + u_{\theta2}^e) \\ = m_\theta^e \ddot{\theta}_1 \end{aligned} \quad [\text{B-3}]$$

Summation of moments for building B2:

$$\begin{aligned} -k_\theta^e u_{\theta2}^e - \frac{6EI}{l_e^2} (u_{y1}^e - u_{y2}^e) - \frac{4EI}{l_e} u_{\theta2}^e - \frac{2EI}{l_e} u_{\theta1}^e - \frac{6EI}{l_e^2} b (u_{\theta1}^e + u_{\theta2}^e) \\ - \frac{12EI}{l_e^3} b (u_{y1}^e - u_{y2}^e) - \frac{6EI}{l_e^2} b (u_{\theta1}^e + u_{\theta2}^e) - \frac{12EI}{l_e^3} b^2 (u_{\theta1}^e + u_{\theta2}^e) \\ = m_\theta^e \ddot{\theta}_2 \end{aligned} \quad [\text{B-4}]$$

$$\begin{aligned} m_y^e \ddot{u}_{y1}^e + \left(k_y^e + \frac{12EI}{l_e^3} \right) u_{y1}^e - \frac{12EI}{l_e^3} u_{y2}^e + \left(\frac{12EI}{l_e^3} b + \frac{6EI}{l_e^2} \right) u_{\theta1}^e \\ + \left(\frac{12EI}{l_e^3} b + \frac{6EI}{l_e^2} \right) u_{\theta2}^e = 0 \end{aligned} \quad [\text{B-5}]$$

$$\begin{aligned} m_y^e \ddot{u}_{y2}^e - \frac{12EI}{l_e^3} u_{y1}^e + \left(k_y^e + \frac{12EI}{l_e^3} \right) u_{y2}^e - \left(\frac{12EI}{l_e^3} b + \frac{6EI}{l_e^2} \right) u_{\theta1}^e \\ - \left(\frac{12EI}{l_e^3} b + \frac{6EI}{l_e^2} \right) u_{\theta2}^e = 0 \end{aligned} \quad [\text{B-6}]$$

$$\begin{aligned}
m_{\theta}^e \ddot{u}_{\theta 1}^e + \left(\frac{12EI}{l_e^3} b + \frac{6EI}{l_e^2} \right) u_{y1}^e - \left(\frac{12EI}{l_e^3} b + \frac{6EI}{l_e^2} \right) u_{y2}^e \\
+ \left(k_{\theta} + \frac{4EI}{l_e} + \frac{12EI}{l_e^2} b + \frac{12EI}{l_e^3} b^2 \right) u_{\theta 1}^e \\
+ \left(\frac{2EI}{l_e} + \frac{12EI}{l_e^2} b + \frac{12EI}{l_e^3} b^2 \right) u_{\theta 2}^e = 0
\end{aligned} \tag{B-7}$$

$$\begin{aligned}
m_{\theta}^e \ddot{u}_{\theta 2}^e + \left(\frac{12EI}{l_e^3} b + \frac{6EI}{l_e^2} \right) u_{y1}^e - \left(\frac{12EI}{l_e^3} b + \frac{6EI}{l_e^2} \right) u_{y2}^e \\
+ \left(\frac{2EI}{l_e} + \frac{12EI}{l_e^2} b + \frac{12EI}{l_e^3} b^2 \right) u_{\theta 1}^e \\
+ \left(k_{\theta} + \frac{4EI}{l_e} + \frac{12EI}{l_e^2} b + \frac{12EI}{l_e^3} b^2 \right) u_{\theta 2}^e = 0
\end{aligned} \tag{B-8}$$

$$k_B = \frac{12EI}{l_e^3} = \frac{12EI}{(l-2b)^3} \tag{B-9}$$

$$m_y^e \ddot{u}_{y1}^e + (k_y^e + k_B) u_{y1}^e - k_B u_{y2}^e + k_B \frac{l}{2} u_{\theta 1}^e + k_B \frac{l}{2} u_{\theta 2}^e = 0 \tag{B-10}$$

$$m_y^e \ddot{u}_{y2}^e - k_B u_{y1}^e - (k_y^e + k_B) u_{y2}^e - k_B \frac{l}{2} u_{\theta 1}^e - k_B \frac{l}{2} u_{\theta 2}^e = 0 \tag{B-11}$$

$$\begin{aligned}
m_{\theta}^e \ddot{u}_{\theta 1}^e + k_B \frac{l}{2} u_{y1}^e - k_B \frac{l}{2} u_{y2}^e + \left[k_{\theta} + \frac{k_B}{3} (l^2 - b l + b^2) \right] u_{\theta 1}^e \\
+ \frac{k_B}{3} \left(\frac{l^2}{2} + b l - b^2 \right) u_{\theta 2}^e = 0
\end{aligned} \tag{B-12}$$

$$\begin{aligned}
m_{\theta}^e \ddot{u}_{\theta 2}^e + k_B \frac{l}{2} u_{y1}^e - k_B \frac{l}{2} u_{y2}^e + \frac{k_B}{3} \left(\frac{l^2}{2} + b l - b^2 \right) u_{\theta 1}^e \\
+ \left[k_{\theta} + \frac{k_B}{3} (l^2 - b l + b^2) \right] u_{\theta 2}^e = 0
\end{aligned} \tag{B-13}$$

Appendix C

Derivation of non-dimensionaled matrix equations for y - θ equations of motion:

$$[m^e]_{y\theta}\{\ddot{u}^e\}_{y\theta} + [k^e]_{y\theta}\{u^e\}_{y\theta} = \{0\} \quad [\text{C-1}]$$

$$\begin{aligned} & \begin{bmatrix} m_y^e & 0 & 0 & 0 \\ 0 & m_y^e & 0 & 0 \\ 0 & 0 & m_\theta^e & 0 \\ 0 & 0 & 0 & m_\theta^e \end{bmatrix} \begin{Bmatrix} \ddot{u}_{y1}^e \\ \ddot{u}_{y2}^e \\ \ddot{u}_{\theta1}^e \\ \ddot{u}_{\theta2}^e \end{Bmatrix} \\ & + k_y^e \begin{bmatrix} \psi_B + 1 & -\psi_B & \psi_B \frac{l}{2} & \psi_B \frac{l}{2} \\ -\psi_B & \psi_B + 1 & -\psi_B \frac{l}{2} & -\psi_B \frac{l}{2} \\ \psi_B \frac{l}{2} & -\psi_B \frac{l}{2} & \frac{k_\theta}{k_y} + \frac{\psi_B}{3}(l^2 - bl + b^2) & \frac{\psi_B}{3}\left(\frac{l^2}{2} + bl - b^2\right) \\ \psi_B \frac{l}{2} & -\psi_B \frac{l}{2} & \frac{\psi_B}{3}\left(\frac{l^2}{2} + bl - b^2\right) & \frac{k_\theta}{k_y} + \frac{\psi_B}{3}(l^2 - bl + b^2) \end{bmatrix} \begin{Bmatrix} u_{y1}^e \\ u_{y2}^e \\ u_{\theta1}^e \\ u_{\theta2}^e \end{Bmatrix} \\ & = \begin{Bmatrix} 0 \\ 0 \\ 0 \\ 0 \end{Bmatrix} \end{aligned} \quad [\text{C-2}]$$

$$\begin{aligned} & \begin{bmatrix} m_y^e & 0 & 0 & 0 \\ 0 & m_y^e & 0 & 0 \\ 0 & 0 & m_y^e \left(\frac{h}{H}\right) r_0^2 & 0 \\ 0 & 0 & 0 & m_y^e \left(\frac{h}{H}\right) r_0^2 \end{bmatrix} \begin{Bmatrix} -\omega^2 u_{y1}^e \\ -\omega^2 u_{y2}^e \\ -\omega^2 u_{\theta1}^e \\ -\omega^2 u_{\theta2}^e \end{Bmatrix} \\ & + k_y^e \begin{bmatrix} \psi_B + 1 & -\psi_B & \psi_B \frac{l}{2} & \psi_B \frac{l}{2} \\ -\psi_B & \psi_B + 1 & -\psi_B \frac{l}{2} & -\psi_B \frac{l}{2} \\ \psi_B \frac{l}{2} & -\psi_B \frac{l}{2} & \frac{k_\theta}{k_y} + \frac{\psi_B}{3}(l^2 - bl + b^2) & \frac{\psi_B}{3}\left(\frac{l^2}{2} + bl - b^2\right) \\ \psi_B \frac{l}{2} & -\psi_B \frac{l}{2} & \frac{\psi_B}{3}\left(\frac{l^2}{2} + bl - b^2\right) & \frac{k_\theta}{k_y} + \frac{\psi_B}{3}(l^2 - bl + b^2) \end{bmatrix} \begin{Bmatrix} u_{y1}^e \\ u_{y2}^e \\ u_{\theta1}^e \\ u_{\theta2}^e \end{Bmatrix} \\ & = \begin{Bmatrix} 0 \\ 0 \\ 0 \\ 0 \end{Bmatrix} \end{aligned} \quad [\text{C-3}]$$

$$\begin{aligned}
& -m_y^e \omega^2 \begin{bmatrix} 1 & 0 & 0 & 0 \\ 0 & 1 & 0 & 0 \\ 0 & 0 & \left(\frac{h}{H}\right) r_0 & 0 \\ 0 & 0 & 0 & \left(\frac{h}{H}\right) r_0 \end{bmatrix} \begin{Bmatrix} u_{y1}^e \\ u_{y2}^e \\ u_{\theta 1}^e \\ u_{\theta 2}^e \end{Bmatrix} \\
& + k_y^e \begin{bmatrix} \psi_B + 1 & -\psi_B & \psi_B \frac{l}{2} & \psi_B \frac{l}{2} \\ -\psi_B & \psi_B + 1 & -\psi_B \frac{l}{2} & -\psi_B \frac{l}{2} \\ \psi_B \frac{l}{2r_0} & -\psi_B \frac{l}{2r_0} & \frac{k_\theta}{k_y r_0} + \frac{\psi_B}{3r_0} (l^2 - bl + b^2) & \frac{\psi_B}{3r_0} \left(\frac{l^2}{2} + bl - b^2\right) \\ \psi_B \frac{l}{2r_0} & -\psi_B \frac{l}{2r_0} & \frac{\psi_B}{3r_0} \left(\frac{l^2}{2} + bl - b^2\right) & \frac{k_\theta}{k_y r_0} + \frac{\psi_B}{3r_0} (l^2 - bl + b^2) \end{bmatrix} \begin{Bmatrix} u_{y1}^e \\ u_{y2}^e \\ u_{\theta 1}^e \\ u_{\theta 2}^e \end{Bmatrix} \quad [\text{C-4}] \\
& = \begin{pmatrix} 0 \\ 0 \\ 0 \\ 0 \end{pmatrix}
\end{aligned}$$

$$\begin{aligned}
& -\frac{m_y^e \omega^2}{k_y^e} \begin{bmatrix} 1 & 0 & 0 & 0 \\ 0 & 1 & 0 & 0 \\ 0 & 0 & \left(\frac{h}{H}\right) & 0 \\ 0 & 0 & 0 & \left(\frac{h}{H}\right) \end{bmatrix} \begin{Bmatrix} u_{y1}^e \\ u_{y2}^e \\ u_{\theta 1}^e r_0 \\ u_{\theta 2}^e r_0 \end{Bmatrix} \\
& + \begin{bmatrix} \psi_B + 1 & -\psi_B & \psi_B \frac{l}{2r_0} & \psi_B \frac{l}{2r_0} \\ -\psi_B & \psi_B + 1 & -\psi_B \frac{l}{2r_0} & -\psi_B \frac{l}{2r_0} \\ \psi_B \frac{l}{2r_0} & -\psi_B \frac{l}{2r_0} & \frac{k_\theta}{k_y r_0^2} + \frac{\psi_B}{3r_0^2} (l^2 - bl + b^2) & \frac{\psi_B}{3r_0^2} \left(\frac{l^2}{2} + bl - b^2\right) \\ \psi_B \frac{l}{2r_0} & -\psi_B \frac{l}{2r_0} & \frac{\psi_B}{3r_0^2} \left(\frac{l^2}{2} + bl - b^2\right) & \frac{k_\theta}{k_y r_0^2} + \frac{\psi_B}{3r_0^2} (l^2 - bl + b^2) \end{bmatrix} \begin{Bmatrix} u_{y1}^e \\ u_{y2}^e \\ u_{\theta 1}^e r_0 \\ u_{\theta 2}^e r_0 \end{Bmatrix} \quad [\text{C-5}] \\
& = \begin{pmatrix} 0 \\ 0 \\ 0 \\ 0 \end{pmatrix}
\end{aligned}$$

$$-\frac{\omega^2}{\omega_{ref}^2} [M] \begin{Bmatrix} u_{y1}^e \\ u_{y2}^e \\ u_{\theta 1}^e r_0 \\ u_{\theta 2}^e r_0 \end{Bmatrix} + [K] \begin{Bmatrix} u_{y1}^e \\ u_{y2}^e \\ u_{\theta 1}^e r_0 \\ u_{\theta 2}^e r_0 \end{Bmatrix} = \begin{pmatrix} 0 \\ 0 \\ 0 \\ 0 \end{pmatrix} \quad [\text{C-6}]$$

$$-\lambda[M][M]^{-1} \begin{Bmatrix} u_{y1}^e \\ u_{y2}^e \\ u_{\theta 1}^e r_0 \\ u_{\theta 2}^e r_0 \end{Bmatrix} + [K][M]^{-1} \begin{Bmatrix} u_{y1}^e \\ u_{y2}^e \\ u_{\theta 1}^e r_0 \\ u_{\theta 2}^e r_0 \end{Bmatrix} = \begin{Bmatrix} 0 \\ 0 \\ 0 \\ 0 \end{Bmatrix} \quad [\text{C-7}]$$

$$-\lambda[I]_{y\theta} \{U^e\}_{y\theta} + [S^e]_{y\theta} \{U^e\}_{y\theta} = \{0\} \quad [\text{C-8}]$$

where:

$$[I]_{y\theta} = \begin{bmatrix} 1 & 0 & 0 & 0 \\ 0 & 1 & 0 & 0 \\ 0 & 0 & 1 & 0 \\ 0 & 0 & 0 & 1 \end{bmatrix} \quad [\text{C-9}]$$

$$[S^e]_{y\theta} = \begin{bmatrix} 1 + \psi_B & -\psi_B & \psi_B \alpha_1 & \psi_B \alpha_1 \\ -\psi_B & 1 + \psi_B & -\psi_B \alpha_1 & -\psi_B \alpha_1 \\ \psi_B \alpha_1 & -\psi_B \alpha_1 & \kappa + \psi_B \alpha_2 & \psi_B \alpha_3 \\ \psi_B \alpha_1 & -\psi_B \alpha_1 & \psi_B \alpha_3 & \kappa + \psi_B \alpha_2 \end{bmatrix} \quad [\text{C-10}]$$

$$\{U^e\}_{y\theta}^T = \left\{ \frac{u_{y1}^e}{D} \quad \frac{u_{y2}^e}{D} \quad \frac{u_{\theta 1}^e H r_0}{D h} \quad \frac{u_{\theta 2}^e H r_0}{D h} \right\} \quad [\text{C-11}]$$

$$\lambda = \frac{\omega^2}{k_y^e / m_y^e} = \frac{\omega^2}{\omega_{y,ref}^2} \quad [\text{C-12}]$$

$$\kappa = \frac{k_\theta^e}{k_y^e r_0^2} \quad [\text{C-13}]$$

$$\alpha_1 = \frac{l}{2 r_0} \quad [\text{C-14}]$$

$$\alpha_2 = \frac{l^2 - bl + b^2}{3 r_0^2} \quad [\text{C-15}]$$

$$\alpha_3 = \frac{\frac{l^2}{2} + bl - b^2}{3 r_0^2} \quad [\text{C-16}]$$

Appendix D

Non-simplified Eigenvalue Output from Maple 13:

$$\lambda_{y,in} = 1 \tag{D-1}$$

$$\lambda_{\theta,out} = \kappa + \psi_B \alpha_2 - \psi_B \alpha_3 \tag{D-2}$$

$$\lambda_{\theta,in} = \psi_B + \frac{1}{2}\kappa + \frac{1}{2}\psi_B \alpha_2 + \frac{1}{2}\psi_B \alpha_3 + \frac{1}{2} \sqrt{\begin{pmatrix} 1 + \psi_B^2 \alpha_3^2 + 4\psi_B^2 + 4\psi_B - 2\psi_B \alpha_2 - 2\kappa \\ -2\psi_B \alpha_3 + 2\psi_B \alpha_3 \kappa + 2\psi_B^2 \alpha_2 \alpha_3 + 2\kappa \psi_B \alpha_2 - 4\kappa \psi_B \\ -4\psi_B^2 \alpha_2 + \kappa^2 + \psi_B^2 \alpha_2^2 - 4\psi_B^2 \alpha_3 + 16\psi_B^2 \alpha_1^2 \end{pmatrix}} \tag{D-3}$$

$$\lambda_{y,out} = \psi_B + \frac{1}{2}\kappa + \frac{1}{2}\psi_B \alpha_2 + \frac{1}{2}\psi_B \alpha_3 + \frac{1}{2} - \frac{1}{2} \sqrt{\begin{pmatrix} 1 + \psi_B^2 \alpha_3^2 + 4\psi_B^2 + 4\psi_B - 2\psi_B \alpha_2 - 2\kappa \\ -2\psi_B \alpha_3 + 2\psi_B \alpha_3 \kappa + 2\psi_B^2 \alpha_2 \alpha_3 + 2\kappa \psi_B \alpha_2 - 4\kappa \psi_B \\ -4\psi_B^2 \alpha_2 + \kappa^2 + \psi_B^2 \alpha_2^2 - 4\psi_B^2 \alpha_3 + 16\psi_B^2 \alpha_1^2 \end{pmatrix}} \tag{D-4}$$

$$\Omega_{y,in} = \sqrt{\lambda_{y,in}} \tag{D-5}$$

$$\Omega_{\theta,out} = \sqrt{\frac{\lambda_{\theta,out} H \omega_y^2}{h \omega_\theta^2}} \tag{D-6}$$

$$\Omega_{\theta,in} = \sqrt{\frac{\lambda_{\theta,in} H \omega_y^2}{h \omega_\theta^2}} \tag{D-7}$$

$$\Omega_{y,out} = \sqrt{\lambda_{y,out}} \tag{D-8}$$